

## **Response to Review Comments**

Re: Manuscript essd-2020-16

*Earth System Science Data*

2020-06-24

Dear Editor,

We would like to thank you and two reviewers for your valuable time and efforts in reviewing our manuscript and providing encouraging and constructive comments. We have revised the manuscript very carefully following all the comments. Below are our responses to each of the comments. The comments are in *italic* and each comment is followed by a response and a tracked change in the revised manuscript.

Please contact us if further information is requested. Thank you in advance.

Yours Sincerely,

Lei Wang

Key Lab. of Tibetan Environmental Changes and Land Surface Processes,

Institute of Tibetan Plateau Research, Chinese Academy of Sciences

No. 16 Lincui Road, Chaoyang District, Beijing 100101, China

Tel: +86-10-84097107      Fax: +86-10-84097079

Email: [wanglei@itpcas.ac.cn](mailto:wanglei@itpcas.ac.cn)

Reviewer #1:

**General comment:**

**Comment 1:** *Overall, I believe this is an excellent work, and will be a highly cited paper. The Upper Brahmaputra River Basin is a very important region to both China and South Asia, and is also an important region for studying the Tibetan Plateau, which is considered as 'The Water Tower of Asia'. The sparse gauge observation data in this region have caused troubles to many scientific studies. The academic community has been expecting a study to integrate various sources of data to develop a better datasets with high spatial and temporal resolutions. This paper fulfils this expectation. The authors used in situ gauge data and hydrological model simulation to evaluate the developed data. The approaches used are rigorous, and the results show the dataset is promising in water related studies. The presentation and literature review are also very good. This paper should be accepted.*

**Response:** Many thanks for your valuable time and efforts in reviewing our manuscript. We do appreciate your positive and encouraging comments.

Review #2:

**General comment:**

**Comment 1:** *In the paper, the authors integrated five satellite/reanalysis data to generate a new precipitation dataset set in the Yarlung Tsangpo basin in South Tibetan Plateau (TP). Actually, the issue is important for the hydrological studies in TP including this study area, but it is also a difficult issue, as there lacks enough observed data. The authors did a good try to generate this precipitation dataset, and it would be useful for the relevant studies in the basin. Overall, I suggest the authors consider more the following issues before its acceptance.*

**Response:** Many thanks for your constructive comments. We have revised the manuscript accordingly following your kind suggestions.

**Detailed Comments:**

**Comment 1:** *The authors assumed that daily precipitation conforms to a normal distribution. However, precipitation data generally follow skew distribution. The reasonability of this assumption should be discussed more.*

**Response:** Of course, the assumption of a normal distribution may lead to uncertainty when analyzing extremely high daily precipitation. Generally, the non-normal (skewed) distribution of precipitation is caused by the zero rainfall events at single observational site (Kumar et al., 2009; Semenov, 2008; Sloughter et al., 2007). We calculated the average values of the observed precipitation from 166 rain gauges to reduce the zero rainfall values. Another associated problem is the quantity and reliability of the data that are used to fit the distribution. If we use different probability distributions to describe the observed time series of daily precipitation, different extreme values may be obtained (Angelidis et al., 2012). This study provides a foundation from which further studies can be carried out to explore these aspects in more detail.

**Change:** We have added discussions and references in the revised manuscript (L360-L366).

*Angelidis, P., Maris, F., Kotsovinos, N., and Hrissanthou, V.: Computation of Drought Index SPI*

*with Alternative Distribution Functions. Water Resour. Manage., 26(9), 2453-2473, 2012.*

*Kumar, M.N., Murthy, C.S., Sai, M.V., and Roy, P.S.: On the use of Standardized Precipitation Index (SPI) for drought intensity assessment. Meteorol. Appl., 16(3), 381-389, 2009.*

*Semenov, M.A.: Simulation of extreme weather events by a stochastic weather generator. Clim. Res., 35(3), 203-212, 2008.*

*Sloughter, J.M., Raftery, A.E., Gneiting, T., and Fraley, C.: Probabilistic Quantitative Precipitation Forecasting Using Bayesian Model Averaging. Mon. Weather Rev., 135(9), 3209-3220, 2007.*

**Comment 2:** *Some contents can be added to discuss more about the altitude effects on the quality of the new precipitation data, especially on the IDW practices, although some discussions have been given in Conclusions.*

**Response:** Thank you for the comments. Generally, these rain gauges were installed at relatively plain area, which may lead to large uncertainty in estimating precipitation (rain or snow) at high mountains, especially in the daily or finer time scales (Ahrens, 2006; Haiden and Pistotnik, 2009). This limitation can be even more severe, due to the orographic effect on precipitation rates, in mountainous regions and transition zones between the low and high altitudes, which will results in the underestimates of the actual basin-wide precipitation (Anders et al., 2006; Hashemi et al., 2020).

Regarding the IDW practices, on the one hand, most of the studied operational precipitation products have already dealt with the altitude effects during data production, and thereby we didn't repeatedly consider the altitude effects when interpolating and integrating these products into 5 km grids with the IDW method. On the other hand, the available gauges (number and distribution) are still far from enough to derive a reasonable spatial distribution of basin-wide altitude gradient for precipitation, due to the complex topography in the study area.

**Change:** We have added discussions and references in the revised manuscript (L347-L356).

*Ahrens, B.: Distance in spatial interpolation of daily rain gauge data. Hydrol. Earth Syst. Sci., 10, 197-208, 2006.*

*Anders, A.M., Roe, G.H., Hallet, B., Montgomery, D.R., and Putkonen, J.: Spatial patterns of precipitation and topography in the himalaya. Geol. Soc. Am. Spec. Pap., 398, 39-53, 2006.*

*Haiden, T., and Pistotnik, G.: Intensity-dependent parameterization of elevation effects in precipitation analysis. Adv. Geosci., 33-38, 2009.*

*Hashemi, H., Fayne, J.V., Lakshmi, V., and Huffman, G.J.: Very high resolution, altitude-corrected, TMPA-based monthly satellite precipitation product over the CONUS. Sci. Data, 7(1), 2020.*

**Comment 3:** *In lines 252-253, it is interesting to find that the weights become smaller with time periods, why? Is it due more reliable quality of the five datasets in recently years? or due to more observed data used? Some contents can be added to simply explain this.*

**Response:** We finally adopted the same weight of each product through the trial-and-error method. Table 1 lists the time ranges of different precipitation products, which are very different and lead to different weights during different periods. As a result, during 1981-1997 (only GLDAS, ITP-Forcing, MERRA2 are available), the weight of each product is 1/3. Similarly, during 1998-2007 and 2008-2016, the weights of each product are 1/4 and 1/5 respectively.

**Table 1.** The precipitation products used in this study.

Precipitation products	Time range	Temporal resolution	Spatial resolution
CMA gridded data	2008-2016	hourly	0.1°×0.1°
GLDAS	1981-2016	3-hour	0.25°×0.25°
ITP-Forcing	1981-2016	3-hour	0.1°×0.1°
MERRA2	1981-2016	hourly	0.5°×0.625°
TRMM	1998-2016	3-hour	0.25°×0.25°

**Change:** We add some description to explain the weight (L252-L257) in the revised manuscript.

**Comment 4:** *In Figure 6, does the P\_int have similar PDF as the CMA? Why?*

**Response:** Yes, the PDF of the P\_int is the closest to that of CMA. Parameters of the normal distribution for the P\_int and the CMA data are also very similar, with a mean value of 77.0 and 75.3 mm, a standard deviation of 62.3 and 62.6 mm, respectively.

The advantage of the CMA product is that it has incorporated more gauge observations (including many unpublished ones of CMA). The short time duration may be the demerit of this product, since it is only available from 2008.

For our newly integrated data, we have incorporated valuable observational gauge

data from Ministry of Water Resources (MWR), China. This greatly helps us to calibrate and validate the  $P_{int}$ .

Therefore, both of two data products have utilized lots of observational information (that provides the ground truth), which leads to the similar PDF.

**Change:** There is no change about this in the manuscript.

**Comment 5:** *This study area should be called “Yarlung Tsangpo” or “Yarlung Zangbo”? please check it.*

**Response:** This area can be called as “Yarlung Zangbo” or “Yarlung Tsangpo”, both of which are acceptable since they are transliterated from Tibetan language (also mentioned in Abstract).

**Changes:** There is no change about this in the manuscript.

# 1 An integration of gauge, satellite and reanalysis precipitation datasets

## 2 for the largest river basin of the Tibetan Plateau

3 Yuanwei Wang<sup>1,3</sup>, Lei Wang<sup>1,2,3\*</sup>, Xiuping Li<sup>1,2</sup>, Jing Zhou<sup>1</sup>, Zhidan Hu<sup>4</sup>

4 <sup>1</sup>Key Laboratory of Tibetan Environmental Changes and Land Surface Processes,

5 Institute of Tibetan Plateau Research, Chinese Academy of Sciences, Beijing, China

<sup>2</sup>CAS Center for Excellence in Tibetan Plateau Earth Sciences, Beijing, China

<sup>3</sup> University of Chinese Academy of Sciences, Beijing, China

<sup>4</sup> Information Center, Ministry of Water Resources, Beijing, China

9

10

11

12

13

14

15

16 Lei Wang Dr Prof

17 Key Lab. of Tibetan

Institute of Tibetan Plateau Research, Chinese Academy of Sciences

48 N-16 Li and B-11 Cl Distributions 100101 Cl

11.  $\overline{1} = 0.110\ldots 107\ldots \overline{1} = 0.110\ldots 107\ldots$

22

23 **Abstract:** As the largest river basin of the Tibetan Plateau, the Upper Brahmaputra  
24 River Basin (also called “Yarlung Zangbo” in Chinese) has profound impacts on the  
25 water security of local and downstream inhabitants. Precipitation in the basin is  
26 mainly controlled by the Indian Summer Monsoon and Westerly, and is the key to  
27 understand the water resources available in the basin; however, due to sparse  
28 observational data constrained by a harsh environment and complex topography, there  
29 remains a lack of reliable information on basin-wide precipitation (there are only nine  
30 national meteorological stations with continuous observations). To improve the  
31 accuracy of basin-wide precipitation data, we integrate various gauge, satellite and  
32 reanalysis precipitation datasets, including GLDAS, ITP-Forcing, MERRA2, TRMM  
33 and CMA datasets, to develop a new precipitation product for the 1981-2016 period  
34 over the Upper Brahmaputra River Basin, at 3-hour and 5-km resolution. The new  
35 product has been rigorously validated at different temporal scales (e.g. extreme events,  
36 daily to monthly variability, and long-term trends) and spatial scales (point- and  
37 basin-scale) with gauge precipitation observations, showing much improved  
38 accuracies compared to previous products. An improved hydrological simulation has  
39 been achieved (low relative bias: -5.94%; highest NSE: 0.643) with the new  
40 precipitation inputs, showing reliability and potential for multi-disciplinary studies.  
41 This new precipitation product is openly accessible at  
42 <https://doi.org/10.5281/zenodo.3711155> (Wang et al., 2020) and, additionally at the  
43 National Tibetan Plateau Data Center (<https://data.tpdc.ac.cn>, login required).  
44

45 **1. Introduction**

46 Precipitation plays a very important role in the research of hydrology, meteorology,  
47 ecology, and even social economics, as it is a critical input factor for various models  
48 (e.g. hydrological and land surface models) (Qi et al., 2016; Wang et al., 2017a; Fang  
49 et al., 2019; Miri et al., 2019; Wang et al., 2019a). Specifically, precipitation is a key  
50 part of the water balance and energy cycle and will directly impact runoff generation  
51 and soil moisture movement (Su et al., 2008). As a result, water resource management  
52 tasks such as flood forecasting and drought monitoring, ecological environment  
53 restoration (e.g. vegetation growth and protection), and many other scientific and  
54 social applications are closely linked with precipitation patterns (Funk et al., 2015).

55 The Tibetan Plateau (TP), known as the highest plateau in the world, is covered by  
56 massive glaciers, snow and permafrost, which significantly affect the hydrological  
57 processes of all the large rivers that are fed by it; the Brahmaputra, the Salween, and  
58 the Mekong, among others. Therefore, it is necessary to explore the hydrological  
59 variations over the TP to achieve efficient utilization and protection of its water  
60 resources and a better understanding of the effects of climate change on the  
61 surrounding region. However, due to the irregular and sparse distribution of national  
62 meteorological stations, particularly in the Upper Brahmaputra (precipitation data  
63 from only nine stations are available, and are sparsely distributed; see Sang et al.,  
64 2016; Cuo et al., 2019), there are large data constraints on research on these  
65 hydrological processes and their responses to climate change. Although there are  
66 many more rain gauges managed by the Ministry of Water Resources (MWR), most

67 of them are located in middle-stream regions and rainfall datasets are only recorded  
68 over short time periods. Simply using the linear mean of these station observations to  
69 calculate variations in precipitation for the entire basin is impractical and prone to  
70 problems (Lu et al., 2015). Accurate spatial distributions of precipitation are  
71 unavailable. This influences the generation of historical runoff data (Mazzoleni et al.,  
72 2019), meaning that the specific contributions of glaciers, snow cover, permafrost and  
73 vegetation to hydrological processes in this area cannot be analyzed and quantified,  
74 posing a threat to regional sustainable development and living conditions (Shen et al.,  
75 2010; Guo et al., 2016; Kidd et al., 2017; Shi et al., 2017; Ruhi et al., 2018; Sun et al.,  
76 2018).

77 A longer time series of spatially consistent and temporally continuous  
78 precipitation products could be used to improve our understanding of feedback  
79 mechanisms between different meteorological and hydrological components,  
80 especially under the background signal of climate change. Various satellite rainfall  
81 products have been widely used in previous studies, such as the National Oceanic and  
82 Atmospheric Administration/Climate Prediction Centre (NOAA/CPC) morphing  
83 technique (CMORPH) (Ferraro et al., 2000; Joyce et al., 2004), and the Tropical  
84 Rainfall Measuring Mission (TRMM) (Huffman et al., 2007). However, there are still  
85 problems in estimating daily (Meng et al., 2014; Bai and Liu, 2018) and extreme  
86 precipitation (Funk et al., 2015; Zhou et al., 2015b; Fang et al., 2019), especially in  
87 mountainous regions with high elevations and fewer ground measurements, such as  
88 the Upper Brahmaputra (Xia et al., 2015; Xu et al., 2017; Qi et al., 2018). Additionally,

89 there are several reanalysis datasets that have been widely used by researchers, such  
90 as the Global Land Data Assimilation System (GLDAS) (Rodell et al., 2004; Zaitchik  
91 et al., 2010; Wang et al., 2011) and the Modern-Era Retrospective analysis for  
92 Research and Applications, Version 2 (MERRA2) dataset (Gelaro et al., 2017; Reichle  
93 et al., 2017a, 2017b). Evaluation of GLDAS data has generally been limited to the  
94 United States and other regions with adequate ground observations (Kato et al., 2007;  
95 Qi et al., 2016). Most studies have focused on evapotranspiration, soil moisture and  
96 groundwater products derived from GLDAS or MERRA2 (Bibi et al., 2019; Deng et  
97 al., 2019; Li et al., 2019a); meanwhile, to the best of our knowledge, there has been  
98 less focus on the evaluation of methods of precipitation estimation and little work on  
99 the corresponding river discharge simulations within the Upper Brahmaputra River  
100 Basin. These precipitation products generally have the advantage of wide and  
101 consistent coverage and have shown great potential in many applications (Li et al.,  
102 2015; Zhang et al., 2017; Fang et al., 2019), but also suffer from large uncertainties  
103 over the Upper Brahmaputra River Basin due to indirect observations, insufficient  
104 gauge calibration, and complex topography (Tong et al., 2014; Yong et al., 2015; Xu  
105 et al., 2017).

106 In this study, we focus on integrating gauge, satellite and reanalysis precipitation  
107 datasets to generate a new dataset over the Upper Brahmaputra, suitable for use in  
108 hydrological simulations and other scientific researches related to climate change. The  
109 remainder of this study is structured as follows. Section 2 briefly describes the study  
110 area, datasets, and methodology used. Section 3 presents and discusses the evaluation

111 results of different products and validates the accuracy and reliability of our integrated  
112 dataset. Then Section 4 is the data availability. Finally, conclusions are given in  
113 Section 5.

114 **2. Materials and Methods**

115 **2.1. Study Area**

116 This study is conducted in Upper Brahmaputra River Basin ( $27^{\circ}$ - $32^{\circ}$ N,  $81^{\circ}$ - $98^{\circ}$ E)  
117 located in the south of the Tibetan Plateau (Figure 1). The Brahmaputra River is an  
118 important part of the whole GBM basin (Ganges, Brahmaputra, Meghna) which  
119 significant influences the natural resources and social development of the Tibetan  
120 Plateau and South Asia. The river is approximately 2,057 km long with a drainage  
121 area of  $240,000 \text{ km}^2$ . The climatic conditions are complicated by the extremely high  
122 altitude and highly varying topography (Wang et al., 2018; Wang et al., 2019b);  
123 elevation varies by up to 6,500 m throughout the study region. Generally, the  
124 intra-annual distribution of precipitation is extremely uneven, with more precipitation  
125 distributed in the warm seasons (Wang et al., 2019a). Since the Indian and East Asian  
126 monsoons bring more water vapor in summer and the westerlies dominate in winter  
127 (Yi et al., 2013; Wang et al., 2018; Li et al., 2019a, 2019b), there is a declining trend  
128 of precipitation from the humid southeast to the arid northwest, on average. In recent  
129 decades, the TP has been experiencing a significant warming trend exceeding that in  
130 the Northern Hemisphere (Liu and Chen, 2000; Yang et al., 2014), which will affect  
131 the generation and distribution of precipitation and influence hydrological processes  
132 throughout the Upper Brahmaputra.

133 **2.2. Datasets**

134 Monthly precipitation data (1981-2016) from nine meteorological stations were  
135 obtained from the China Meteorological Administration (CMA), and daily  
136 precipitation data (May to October in 2014 and 2016) from 166 rain gauges were  
137 accessed through the Ministry of Water Resources (MWR), China (Figure 1). Both of  
138 these are regarded as observed precipitation data. Daily river discharge data at Nuxia  
139 station (Figure 1) are used to assess the simulation performance when forced by  
140 different precipitation products.

141 In this study, we chose five types of satellite and reanalysis precipitation products  
142 (Table 1). We, first, evaluated their performance at detecting precipitation, and second,  
143 integrated them to generate a better product, designed to enhance the strengths of each  
144 product.

145 The three satellite and reanalysis data products, GLDAS, MERRA2 and TRMM,  
146 were acquired from the National Aeronautics and Space Administration (NASA)  
147 website (<https://disc.gsfc.nasa.gov/>). GLDAS ingests satellite- and ground-based  
148 observational data products and applies advanced land surface modeling and data  
149 assimilation techniques (Rodell et al., 2004; Zaitchik et al., 2010; Xia et al., 2019); it  
150 has been widely used for river discharge simulations, groundwater monitoring and  
151 many other fields (Wang et al., 2011; Chen et al., 2013; Qi et al., 2018; Verma and  
152 Katpatal, 2019). MERRA2 is the first long-term global reanalysis dataset to assimilate  
153 space-based observations of aerosols and represent their interactions alongside other  
154 physical processes in the climate system (Marquardt Collow et al., 2016; Reichle et al.,

155 2017a, 2017b), and TRMM is a joint mission between the NASA and the Japan  
156 Aerospace Exploration Agency (JAXA) to study rainfall for weather and climate  
157 research (Xu et al., 2017; Ali et al., 2019; Wang et al., 2019a). The ITP-Forcing  
158 dataset has been developed by the hydrometeorological research group at the Institute  
159 of Tibetan Plateau Research, Chinese Academy of Sciences (He, 2010), and has been  
160 shown to perform well on the TP (Yang et al., 2010; Chen et al., 2011). These data  
161 were downloaded from the Cold and Arid Regions Science Data Center  
162 (<http://westdc.westgis.ac.cn/>).

163 **2.3. Methods**

164 In this study, because of the different spatial resolutions of different products, we  
165 extracted the precipitation values from each product according to the locations of the  
166 gauges to generate product-gauge data pairings for evaluation. Where there are at least  
167 two gauges in the pixel of one product, we used the average value of the gauges to  
168 evaluate the performance of the corresponding precipitation product data.

169 To ensure the consistency of different products, we interpolated all the products  
170 into the same 5 km spatial resolution grid using the inverse distance weighted (IDW)  
171 method (Ma et al., 2019; Qiao et al., 2019; Sangani et al., 2019) and calculated them  
172 at 3-hourly resolution. Due to its good performance on the TP, we then used the  
173 ITP-Forcing data (1981-2016) to derive the multi-year mean 3-hour data as  
174 background climatological precipitation. Then, the precipitation anomalies between  
175 CMA, GLDAS, ITP-Forcing, MERRA2, TRMM and the background were calculated  
176 3-hourly, using:

$$\begin{aligned}
\varepsilon_c &= P_C - P_B \\
\varepsilon_g &= P_G - P_B \\
\varepsilon_i &= P_I - P_B \\
\varepsilon_m &= P_M - P_B \\
\varepsilon_t &= P_T - P_B
\end{aligned} \tag{1}$$

177 where  $P_B$ ,  $P_C$ ,  $P_G$ ,  $P_I$ ,  $P_M$ ,  $P_T$  represent the background precipitation and different  
 178 products, respectively, and  $\varepsilon$  denotes the corresponding precipitation anomalies.  
 180 Considering different weights for these anomalies, we combined the background  
 181 precipitation with these anomalies,

$$P\_int = P_B + w_1\varepsilon_c + w_2\varepsilon_g + w_3\varepsilon_i + w_4\varepsilon_m + w_5\varepsilon_t \tag{2}$$

183 where  $w$  represents the weight for each anomaly and  $P\_int$  refers to the new integrated  
 184 precipitation at 5 km and 3-hourly resolution.

185 After  $P\_int$  was acquired, we corrected its probability distribution function (PDF)  
 186 based on the rain gauges, and undertook several validation steps for spatial  
 187 distribution and at different time scales (e.g. extreme events, seasonal to inter-annual  
 188 variability, and long-term trends). At the same time, we also analyzed the changing  
 189 trend over the 36 years, and the extremely high precipitation events during the warm  
 190 months in 2014 and 2016. In order to identify the extreme events, we first assumed  
 191 that daily precipitation conforms to a normal distribution. From this we calculated a  
 192 threshold, above which the probability of precipitation values occurring is less than  
 193 0.05 (e.g. Fang et al., 2019 use 0.1). We considered events with precipitation values  
 194 above this threshold as extreme events.

$$P(\text{precipitation} \geq \text{threshold}) \leq 0.05 \tag{3}$$

196 where  $P$  denotes the probability. Finally, based on the observed discharge data at

197 Nuxia Station, we compared the simulated daily discharges (normalized) from 2008 to  
 198 2016 using a water and energy budget-based distributed hydrological model  
 199 (WEB-DHM) to check the accuracy and reliability of our integrated precipitation.  
 200 Evaluation criteria used in the discharge error assessment include relative bias (RB)  
 201 and the Nash-Sutcliffe coefficient of efficiency (NSE).

$$202 Q_{normalized} = \frac{Q - \min Q_{obs}}{\max Q_{obs} - \min Q_{obs}} \quad (4)$$

$$203 RB = \frac{\sum_{i=1}^n Q_{sim} - \sum_{i=1}^n Q_{obs}}{\sum_{i=1}^n Q_{obs}} \times 100\% \quad (5)$$

$$204 NSE = 1 - \frac{\sum_{i=1}^n (Q_{obs} - Q_{sim})^2}{\sum_{i=1}^n (Q_{obs} - \bar{Q}_{obs})^2} \quad (6)$$

205 Where  $Q_{normalized}$ ,  $Q_{obs}$ ,  $Q_{sim}$  represent the normalized discharge, observed discharge,  
 206 and simulated discharge, respectively. The perfect value of  $RB$  is 0 and that of  $NSE$  is  
 207 1. More information about this model can be found in many studies (Wang et al., 2009;  
 208 Wang and Koike, 2009; Xue et al., 2013; Zhou et al., 2015a; Wang et al., 2016; Wang  
 209 et al., 2017a). Figure 2 shows the flowchart of this study and Figure 3 presents the  
 210 final spatial distribution of our integrated product.

211 **3. Results and Discussion**

212 **3.1. Evaluation of precipitation products at the basin and grid scale**

213 Figures 4 and 5 analyze the overall regime of different precipitation products at  
 214 the basin scale. Figure 4 is the spatial distribution in warm (May to Oct.) and cold

215 (Nov. to Apr.) months, and Figure 5 presents the time series of basin-averaged annual  
216 and monthly precipitation values. The spatial pattern indicates that more precipitation  
217 occurs in warm seasons and less in cold seasons. During the warm months, GLDAS  
218 and TRMM present obvious regional differences between upstream and downstream,  
219 while CMA gridded data show the lesser values in the upstream source region. In the  
220 cold seasons, all products present almost the same pattern, among which MERRA2  
221 gives the lowest precipitation values.

222 For annual precipitation, CMA, ITP-Forcing and MERRA2 show similar  
223 characteristics (annual mean value: 615 mm, 550 mm and 506 mm, respectively),  
224 while GLDAS and TRMM are 789 mm and 757 mm, respectively. There are also  
225 significant ( $p < 0.01$ ) increasing trends in annual precipitation of GLDAS,  
226 ITP-Forcing, and MERRA2 (6.42, 3.28, 4.68 mm/year, respectively) over the 36 years  
227 of the data. For monthly precipitation, GLDAS and TRMM greatly overestimate  
228 summer precipitation compared to the others, which explains why these two products  
229 give anomalously high annual values (nearly 200 mm greater than the other three data  
230 products). On the other hand, the monthly variations indicate that the intra-annual  
231 distribution of precipitation is extremely uneven.

232 Figures 6 and 7 compare the accuracy of monthly rainfall from different products  
233 at the grid scale. Due to the coarse spatial resolution of MERRA2 ( $0.5^\circ \times 0.625^\circ$ ), there  
234 are fewer product-gauge data pairings available for evaluation. All the products show  
235 similar correlation relationships with the observations, with most rain gauges  
236 overestimating monthly precipitation (Figure 7). The highest correlation coefficient is

237 0.63 (MERRA2) and the lowest is 0.51 (GLDAS). The PDFs, however, show  
238 different characteristics (Figure 6). The CMA data are more consistent with the gauge  
239 data, while GLDAS and TRMM exhibit clear overestimations. As for ITP-Forcing, its  
240 precipitation is more concentrated on the average value, as indicated by the narrow  
241 curve.

242 **3.2. Integration of precipitation products and validation of  $P_{int}$**

243 **3.2.1. Integration of precipitation products and validation against different time  
244 series**

245 Figure 3 presents the spatial distribution of annual and seasonal precipitation  
246 estimated by our integrated dataset, which shows a declining trend from the southeast  
247 to northwest. Figure 5 then compares the monthly and annual precipitation calculated  
248 from our integrated dataset with the satellite and reanalysis products. As discussed in  
249 Section 2.3, we interpolated all the products into a spatial resolution of 5 km using the  
250 IDW method, and calculated them at a temporal resolution of 3 hours. Comparing  
251 different weights for the anomalies mentioned in Equation 2, we finally adopted the  
252 same weight for each product [and the sum of the weights is 1](#) ( $w = 1/3$  from 1981 to  
253 1997;  $w = 0.25$  from 1998 to 2007;  $w = 0.2$  from 2008 to 2016) to develop the new  
254 product. [We made the integrated precipitation data using equal weights essentially](#)  
255 [according to the number of available precipitation products at different time periods](#)  
256 [\(Table 1\).](#) Then we corrected the PDF of the newly integrated data based on the rain  
257 [gauge observations \(Figure 6\).](#)

258 After  $P_{int}$  was derived, we first validated its performance against short time

259 series (Figure 8).  $P_{int}$  shows optimal performance at detecting daily precipitation  
260 with the correlation coefficients of 0.43 in 2014 and 0.55 in 2016. In 2014, the  
261 average bias is 0.20 mm and the root mean square error (RMSE) is 4.18 mm.  $P_{int}$   
262 successfully captures the daily variation of precipitation except for late September and  
263 early October. For 2016, the average bias and RMSE are -0.006 mm and 2.62 mm,  
264 respectively, much better than those for 2014.

265 We then check the spatial distribution of  $P_{int}$  from May to October in 2014 and  
266 2016 (Figure 9). Every rain gauge is compared with its corresponding grid in  $P_{int}$  to  
267 explore the spatial heterogeneity.  $P_{int}$  well reproduces the precipitation pattern  
268 described by less rain in the upstream (western) regions and more rain in the  
269 downstream (eastern) regions. Meanwhile, abundant rainfall occurs in summer,  
270 particularly for July.

271 Building on this, further validation was undertaken against a long time series. We  
272 chose the average monthly precipitation from the nine meteorological stations as the  
273 evaluation standard against which to assess  $P_{int}$  (Figure 10). The PDF of  $P_{int}$  is  
274 consistent with that of the station data, which indicates that the mean value and  
275 standard deviation of  $P_{int}$  are much closer to the observed value (Figure 10a).  
276 Similar to the short time series, the average bias (-4.50 mm) and the RMSE (13.6 mm),  
277 especially with respect to the correlation coefficient (0.96), prove that the  $P_{int}$  is  
278 applicable and reliable.

279 **3.2.2. Trend and extreme events analysis compared across different precipitation**  
280 **products**

281 The trend analysis (Figure 11) over 36 years indicates that there are different  
282 patterns of precipitation in different seasons and different regions. In summer, there  
283 are more complicated trends, as the variations between up and down stream differ  
284 greatly. On the contrary, trends of winter precipitation values over most of the study  
285 region vary by merely  $\pm 2$  mm/year, illustrating that precipitation in winter generally  
286 remains unchanged or experiences minimal change. To find if  $P_{int}$  is able to reflect  
287 the true varying trend, we added a comparison between meteorological stations  
288 (triangles in Figure 11 and their direction represent the true trend) and precipitation  
289 products. For observed annual precipitation, all the stations give an insignificant  
290 increasing trend, except for Bomi station, which is located in the easternmost part of  
291 the study region. For seasonal precipitation, different stations present different  
292 patterns. As a result,  $P_{int}$  appears to reflect the changing pattern of more stations  
293 than any other product, with the exception of the ITP-Forcing dataset on an annual  
294 timescale or over autumn (Figure 12).

295 We notice that there is increasing trend in annual precipitation almost in the  
296 whole basin for  $P_{int}$ ; only precipitation in the midstream area near the Himalaya  
297 mountains and small part of the upstream region are decreasing. Moreover, the  
298 majority of the increased precipitation in the downstream regions occurs over spring  
299 and summer, with only slight changes found in autumn and winter.

300 After the volume, the spatial distribution, and the trend of  $P_{int}$  at different time  
301 scales were completely verified, we continued to inspect if  $P_{int}$  could capture the  
302 extreme events from May to October in 2014 and 2016 according to the rain gauge

303 data (Figure 13). There are 27 days in total (19 days in 2014 and 8 days in 2016)  
304 when extremely high daily precipitation occurred. All the products are comparable  
305 with each other in underestimating the frequency of extreme events. Nine days are  
306 identified out of the  $P_{int}$  data, lesser only to the number of days detected by  
307 ITP-Forcing (11 days).

308 **3.2.3. Evaluation of daily discharges simulated by different precipitation  
309 products**

310 All the comparison and validation steps undertaken above support the accuracy  
311 and reliability of our integrated dataset. Furthermore, Figure 14 indicates the superior  
312 suitability and application of  $P_{int}$  in hydrological simulation and investigation, with  
313 an RB of -5.94% and an NSE of 0.643 (the highest). We simulate the daily discharge  
314 of Nuxia station using the various precipitation datasets as the input with the same  
315 initial conditions and physical parameters. All products overestimate the daily  
316 discharge, except for  $P_{int}$  (-5.94%) and MERRA2 (-2.24%). In terms of NSE,  $P_{int}$   
317 (0.643), ITP-Forcing (0.543) and MERRA2 (0.544) are higher than others, explaining  
318 their better simulation performance. GLDAS and TRMM offer the worst performance  
319 in discharge simulation, which is consistent with their overestimation of precipitation  
320 in summer (Figure 5). This indicates that these datasets should be corrected when  
321 undertaking hydrological research over the Upper Brahmaputra.

322 **4. Data availability**

323 This high spatiotemporal resolution (5km, 3h) precipitation dataset over the  
324 Upper Brahmaputra River Basin from 1981 to 2016 is freely available at

325 <https://doi.org/10.5281/zenodo.3711155> (Wang et al., 2020), which can be  
326 downloaded in TXT format.

327 **5. Conclusion**

328 In order to acquire suitable and accurate precipitation datasets which are helpful  
329 in hydrology, meteorology and other scientific research over the Upper Brahmaputra,  
330 we produced a new precipitation product by integrating gauge, satellite and reanalysis  
331 precipitation datasets to reduce the uncertainties associated with a single product and  
332 limitation of few observation stations. Our integrated dataset performs better than the  
333 input datasets in estimating daily and monthly precipitation, describing the spatial  
334 heterogeneity, capturing variation trends and extreme events and simulating river  
335 discharges. Furthermore, it is successful in reproducing daily precipitation variation,  
336 with smaller average biases (0.2 mm in 2014 and -0.006 mm in 2016) and RMSE  
337 values (4.18 mm in 2014 and 2.62 mm in 2016). Monthly precipitation shows higher  
338 correlation coefficients with the in-situ data for various time series (0.69 for all the  
339 rain gauges in the warm months of 2014 and 2016; 0.86 for the nine meteorological  
340 stations over 1981-2016). This high spatio-temporal resolution assures us that we can  
341 use this new dataset to explore more detailed physical processes and further  
342 understand the impacts of climate change on the water resources of the Upper  
343 Brahmaputra River Basin, and we are confident that our precipitation dataset will  
344 greatly assist future research in this basin.

345 With this in mind, we note some aspects of this study that deserve further  
346 consideration. The effect of altitude on precipitation has not been taken into account

347 in the development of this dataset. The 166 rain gauges used in this paper, are all  
348 located at the elevations above 3500 m, except for several eastern gauges. Generally,  
349 these gauges were installed at relatively plain area, which may lead to large  
350 uncertainty in estimating precipitation (rain or snow) at high mountains, especially in  
351 the daily or finer time scales (Ahrens, 2006; Haiden and Pistotnik, 2009). This  
352 limitation can be even more severe, due to the orographic effect on precipitation rates,  
353 in mountainous regions and transition zones between the low and high altitudes,  
354 which will result in the underestimates of the actual basin-wide precipitation (Anders  
355 et al., 2006; Hashemi et al., 2020). Increasing the density and the distribution area of  
356 observational stations can directly weaken this altitude effects. We also note  
357 uncertainties that may arise from the re-gridding of the remotely sensed datasets in  
358 order to pair with the in-situ gauge data. In addition, the assumption of normal  
359 distribution when analyzing extremely high daily precipitation can also lead to  
360 uncertainty. Generally, the non-normal (skewed) distribution of precipitation is caused  
361 by the zero rainfall events at single site (Kumar et al., 2009; Semenov, 2008;  
362 Sloughter et al., 2007). An associated problem is the quantity and reliability of the  
363 data used to fit the distribution. Different probability distributions are used to describe  
364 the observed time series of daily precipitation, then different extreme values may be  
365 obtained (Angelidis et al., 2012). This study provides a foundation from which further  
366 studies can be carried out to explore these aspects in more detail.

367 In the future, more studies are needed to validate the method and data in regions  
368 with complex topography and climatic conditions, and to further improve the retrieval

369 algorithm. This will greatly benefit hydrological applications, especially in areas with  
370 sparse and irregular observation networks. Furthermore, no products used in this  
371 study accurately represent extreme precipitation events, thus, it is necessary to  
372 improve the ability of all of these products to capture extreme events.

373 **Acknowledgments**

374 This study was financially supported by the National Natural Science Foundation  
375 of China (Grant No. 91747201) and the Strategic Priority Research Program of  
376 Chinese Academy of Sciences (Grant No. XDA20060202 and XDA19070301). Jing  
377 Zhou was supported by the National Natural Science Foundation of China (Grant No.  
378 41771089). The Shuttle Radar Topographic Mission (SRTM) Digital Elevation Model  
379 (DEM), with a ground resolution of 30 m, is available from the United States  
380 Geological Survey's (USGS) web portal ([www.earthexplorer.usgs.gov](http://www.earthexplorer.usgs.gov)). We would  
381 also like to thank NASA for different precipitation data including GLDAS, MERRA2,  
382 TRMM (<https://disc.gsfc.nasa.gov/>). Lastly, we are pleased to acknowledge the  
383 anonymous reviewers and editor's valuable comments and suggestions to improve  
384 this manuscript.

385 **Conflicts of Interest**

386 The authors declare no conflicts of interest.

387 **References**

388 Ahrens, B.: Distance in spatial interpolation of daily rain gauge data. *Hydrol. Earth  
389 Syst. Sci.*, 10, 197-208, 2006.  
390 Ali, S., Tong, D., Xu, Z., Henchiri, M., Wilson, K., Shi, S., and Zhang, J.:

391 Characterization of drought monitoring events through MODIS- and  
392 TRMM-based DSI and TVDI over south Asia during 2001–2017, Environ. Sci.  
393 Pollut. Res., 26(32), 33568-33581, 2019.

394 Anders, A.M., Roe, G.H., Hallet, B., Montgomery, D.R., and Putkonen, J.: Spatial  
395 patterns of precipitation and topography in the himalaya. Geol. Soc. Am. Spec.  
396 Pap., 398, 39-53, 2006.

397 Angelidis, P., Maris, F., Kotsovinos, N., and Hrissanthou, V.: Computation of  
398 Drought Index SPI with Alternative Distribution Functions. Water Resour.  
399 Manage., 26(9), 2453-2473, 2012.

400 Bai, P., and Liu, X.: Evaluation of Five Satellite-Based Precipitation Products in Two  
401 Gauge-Scarce Basins on the Tibetan Plateau, Remote Sens., 10(8), 1316, 2018.

402 Bibi, S., Wang, L., Li, X., Zhang, X., and Chen, D.: Response of groundwater storage  
403 and recharge in the Qaidam Basin (Tibetan Plateau) to climate variations from  
404 2002 to 2016, J. Geophys. Res.: Atmos., 124(17-18), 9918-9934, 2019.

405 Chen, Y., Yang, K., He, J., Qin, J., Shi, J., Du, J., and He, Q.: Improving land surface  
406 temperature modeling for dry land of China, J. Geophys. Res.: Atmos., 116(D20),  
407 2011.

408 Chen, Y., Yang, K., Qin, J., Zhao, L., Tang, W., and Han, M.: Evaluation of AMSR-E  
409 retrievals and GLDAS simulations against observations of a soil moisture  
410 network on the central Tibetan Plateau, J. Geophys. Res.: Atmos., 118(10),  
411 4466-4475, 2013.

412 Cuo, L., Li, N., Liu, Z., Ding, J., Liang, L., Zhang, Y., and Gong, T.: Warming and

413 human activities induced changes in the Yarlung Tsangpo basin of the Tibetan  
414 plateau and their influences on streamflow, *J. Hydrol.: Regional Studies*, 25,  
415 100625, 2019

416 Deng, M., Meng, X., Li, Z., Lyv, Y., Lei, H., Zhao, L., Zhao, S., Ge, J., and Jing, H.:  
417 Responses of soil moisture to regional climate change over the Three Rivers  
418 Source Region on the Tibetan plateau, *Int. J. Climatol.*, 1-15, 2019.

419 Fang, J., Yang, W., Luan, Y., Du, J., Lin, A., and Zhao, L.: Evaluation of the TRMM  
420 3B42 and GPM IMERG products for extreme precipitation analysis over China,  
421 *Atmos. Res.*, 223, 24-38, 2019.

422 Ferraro, R.R., Weng, F., Grody, N.C., and Zhao, L.: Precipitation characteristics over  
423 land from the NOAA-15 AMSU sensor, *Geophys. Res. Lett.*, 27(17), 2669-2672,  
424 2000.

425 Funk, C., Peterson, P., Landsfeld, M., Pedreros, D., Verdin, J., Shukla, S., Husak, G.,  
426 Rowland, J., Harrison, L., Hoell, A., and Michaelsen, J.: The climate hazards  
427 infrared precipitation with stations-a new environmental record for monitoring  
428 extremes, *Sci. Data*, 2(1), 1-21, 2015.

429 Gelaro, R., McCarty, W., Suárez, M.J., Todling, R., Molod, A., Takacs, L., Randles,  
430 C.A., Darmenova, A., Bosilovich, M.G., Reichle, R., Wargan, K., Coya, L.,  
431 Cullather, R., Draper, C., Akella, S., Buchard, V., Conaty, A., Silva, A.M., Gu,  
432 W., Kima, G-K., Koster, R., Lucchesi, R., Merkova, D., Nielsen, J.E., Partyka,  
433 G., Pawson, S., Putman, W., Riendecker, M., Schubert, S.D., Sienkiewicz, M.,  
434 and Zhao, B.: The modern-era retrospective analysis for research and

435 applications, version 2 (MERRA-2), *J. Clim.*, 30(14), 5419-5454, 2017.

436 Guo, H., Chen, S., Bao, A., Behrangi, A., Hong, Y., Ndayisaba, F., Hu, J., and  
437 Stepanian, P.M.: Early assessment of integrated multi-satellite retrievals for  
438 global precipitation measurement over China, *Atmos. Res.*, 176, 121-133, 2016.

439 Haiden, T., and Pistotnik, G.: Intensity-dependent parameterization of elevation  
440 effects in precipitation analysis. *Adv. Geosci.*, 33-38, 2009.

441 Hashemi, H., Fayne, J.V., Lakshmi, V., and Huffman, G.J.: Very high resolution,  
442 altitude-corrected, TMPA-based monthly satellite precipitation product over the  
443 CONUS. *Sci. Data*, 7(1), 2020.

444 He, J.: Development of surface meteorological dataset of China with high temporal  
445 and spatial resolution, Master dissertation, Institute of Tibetan Plateau Research,  
446 Chinese Academy of Science, 2010.

447 Huffman, G.J., Adler, R.F., Rudolf, B., Schneider, U., and Keehn, P.R.: Global  
448 precipitation estimates based on a technique for combining satellite-based  
449 estimates, rain gauge analysis, and NWP model precipitation information, *J.*  
450 *Clim.*, 8(5), 1284-1295, 1995.

451 Huffman, G.J., Bolvin, D.T., Nelkin, E.J., Wolff, D.B., Adler, R.F., Gu, G., Hong, Y.,  
452 Bowman, K.P., and Stocker, E.F.: The TRMM multisatellite precipitation  
453 analysis (TMPA): Quasi-global, multiyear, combined-sensor precipitation  
454 estimates at fine scales, *J. Hydrometeorol.*, 8(1), 38-55, 2007.

455 Joyce, R.J., Janowiak, J.E., Arkin, P.A., and Xie, P.: CMORPH: A method that  
456 produces global precipitation estimates from passive microwave and infrared

457 data at high spatial and temporal resolution, *J. Hydrometeorol.*, 5(3), 487-503,  
458 2004.

459 Kato, H., Rodell, M., Beyrich, F., Cleugh, H., Gorsel, E.V., Liu, H., and Meyers, T.P.:  
460 Sensitivity of land surface simulations to model physics, land characteristics, and  
461 forcings, at four CEOP sites, *J. Meteorol. Soc. Jpn.*, 85, 187-204, 2007.

462 Kidd, C., Becker, A., Huffman, G.J., Muller, C.L., Joe, P., Skofronick-Jackson, G.,  
463 and Kirschbaum, D.B.: So, how much of the Earth's surface is covered by rain  
464 gauges?, *Bull. Am. Meteorol. Soc.*, 98(1), 69-78, 2017.

465 **Kumar, M.N., Murthy, C.S., Sai, M.V., and Roy, P.S.: On the use of Standardized**  
466 **Precipitation Index (SPI) for drought intensity assessment. *Meteorol. Appl.*,**  
467 **16(3), 381-389, 2009.**

468 Li, X., Long, D., Han, Z., Scanlon, B.R., Sun, Z., Han, P., and Hou, A.:  
469 Evapotranspiration Estimation for Tibetan Plateau Headwaters using Conjoint  
470 Terrestrial and Atmospheric Water Balances and Multisource Remote Sensing,  
471 *Water Resour. Res.*, 55, <https://doi.org/10.1029/2019WR025196>, 2019a.

472 Li, X., Long, D., Huang, Q., Han, P., Zhao, F., and Wada, Y.:  
473 High-temporal-resolution water level and storage change data sets for lakes on  
474 the Tibetan Plateau during 2000–2017 using multiple altimetric missions and  
475 Landsat-derived lake shoreline positions, *Earth Syst. Sci. Data*, 11(4), 1603-1627,  
476 2019b.

477 Li, Z., Yang, D., Gao, B., Jiao, Y., Hong, Y., and Xu, T.: Multiscale hydrologic  
478 applications of the latest satellite precipitation products in the Yangtze River

479 Basin using a distributed hydrologic model, *J Hydrometeorol.*, 16(1), 407-426,  
480 2015.

481 Liu, X., and Chen, B.: Climatic warming in the Tibetan Plateau during recent decades,  
482 *Int. J. Climatol.*, 20(14), 1729-1742, 2000.

483 Lu, N., Trenberth, K.E., Qin, J., Yang, K., and Yao, L.: Detecting long-term trends in  
484 precipitable water over the Tibetan Plateau by synthesis of station and MODIS  
485 observations, *J. Clim.*, 28(4), 1707-1722, 2015.

486 Ma, J., Ding, Y., Cheng, J.C.P., Jiang, F., and Wan, Z.: A temporal-spatial  
487 interpolation and extrapolation method based on geographic Long Short-Term  
488 Memory neural network for PM 2.5, *J. Cleaner Prod.*, 237, 117729, 2019.

489 Marquardt Collow, A.B., Bosilovich, M.G., and Koster, R.D.: Large-scale influences  
490 on summertime extreme precipitation in the northeastern United States, *J.*  
491 *Hydrometeorol.*, 17(12), 3045-3061, 2016.

492 Mazzoleni, M., Brandimarte, L., and Amaranto, A.: Evaluating precipitation datasets  
493 for large-scale distributed hydrological modelling, *J. Hydrol.*, 578, 124076, 2019.

494 Meng, J., Li, L., Hao, Z., Wang, J., and Shao, Q.: Suitability of TRMM satellite  
495 rainfall in driving a distributed hydrological model in the source region of  
496 Yellow River, *J. Hydrol.*, 509, 320-332, 2014.

497 Miri, M., Masoudi, R., and Raziei, T.: Performance Evaluation of Three  
498 Satellites-Based Precipitation Data Sets Over Iran, *J. Indian Soc. Remot.*, 47(12),  
499 2073-2084, 2019.

500 Qi, W., Liu, J., and Chen, D.: Evaluations and improvements of GLDAS2.0 and

501 GLDAS2.1 forcing data's applicability for basin scale hydrological simulations  
502 in the Tibetan Plateau, *J. Geophys. Res.: Atmos.*, 123(23), 13,128-13,148, 2018.

503 Qi, W., Zhang, C., Fu, G., Sweetapple, C., and Zhou, H.: Evaluation of global  
504 fine-resolution precipitation products and their uncertainty quantification in  
505 ensemble discharge simulations, *Hydrol. Earth Syst. Sci.*, 20(2), 903-920, 2016.

506 Qi, W., Zhang, C., Fu, G., and Zhou H.: Global Land Data Assimilation System data  
507 assessment using a distributed biosphere hydrological model, *J. Hydrol.*, 528,  
508 652-667, 2015.

509 Qiao, P., Li, P., Cheng, Y., Wei, W., Yang, S., Lei, M., and Chen, T.: Comparison of  
510 common spatial interpolation methods for analyzing pollutant spatial  
511 distributions at contaminated sites, *Environ. Geochem. Health*, 41, 2709-2730,  
512 2019.

513 Rasouli, K., Pomeroy, J.W., Janowicz, J.R., Williams, T.J., and Carey, S.K.: A  
514 long-term hydrometeorological dataset (1993–2014) of a northern mountain  
515 basin: Wolf Creek Research Basin, Yukon Territory, Canada, *Earth Syst. Sci.*  
516 *Data*, 11(1), 89-100, 2019.

517 Reichle, R.H., Draper, C.S., Liu, Q., Girotto, M., Mahanama, S.P.P., Koster, R.D.,  
518 and De Lannoy, G.J.M.: Assessment of MERRA-2 land surface hydrology  
519 estimates, *J. Clim.*, 30(8), 2937-2960, 2017a.

520 Reichle, R.H., Liu, Q., Koster, R.D., Draper, C.S., Mahanama, S.P.P., and Partyka,  
521 G.S.: Land surface precipitation in MERRA-2, *J. Clim.*, 30(5), 1643-1664,  
522 2017b.

523 Roca, R., Alexander, L.V., Potter, G., Bador, M., Juca, R., Contractor, S., Bosilovich,  
524 M.G., and Cloche, S.: FROGS: a daily  $1^\circ \times 1^\circ$  gridded precipitation database of  
525 rain gauge, satellite and reanalysis products, *Earth Syst. Sci. Data*, 11(3),  
526 1017-1035, 2019.

527 Rodell, M., Houser, P.R., Jambor, U., Gottschalck, J., Mitchell, K., Meng, C-J.,  
528 Arsenault, K., Cosgrove, B., Radakovich, J., Bosilovich, M., Entin, J.K., Walker,  
529 J.P., Lohmann, D., and Toll, D.: The Global Land Data Assimilation System,  
530 *Bull. Am. Meteorol. Soc.*, 85(3), 381-394, 2004.

531 Rodell, M., McWilliams, E.B., Famiglietti, J.S., Beaudoin, H.K., and Nigro, J.:  
532 Estimating evapotranspiration using an observation based terrestrial water budget,  
533 *Hydrol. Processes*, 25(26), 4082-4092, 2011.

534 Ruhi, A., Messager, M.L., and Olden, J.D.: Tracking the pulse of the Earth's fresh  
535 waters, *Nature Sustainability*, 1(4), 198-203, 2018.

536 Sang, Y., Singh, V.P., Gong, T., Xu, K., Sun, F., Liu, C., Liu, W., and Chen, R.:  
537 Precipitation variability and response to changing climatic condition in the  
538 Yarlung Tsangpo River basin, China, *J. Geophys. Res.: Atmos.*, 121, 8820–8831,  
539 doi:10.1002/2016JD025370, 2016.

540 Sangani, M.F., Khojasteh, D.N., and Owens, G.: Dataset characteristics influence the  
541 performance of different interpolation methods for soil salinity spatial mapping,  
542 *Environ. Monit. Assess.*, 191(11), 684, 2019.

543 Savtchenko, A.K., Huffman, G., and Vollmer, B.: Assessment of precipitation  
544 anomalies in California using TRMM and MERRA data, *J. Geophys. Res.*:

545 Atmos., 120(16), 8206-8215, 2015.

546 Semenov, M.A.: Simulation of extreme weather events by a stochastic weather  
547 generator. *Clim. Res.*, 35(3), 203-212, 2008.

548 Shen, G., Chen, N., Wang, W., and Chen Z.: WHU-SGCC: a novel approach for  
549 blending daily satellite (CHIRP) and precipitation observations over the Jinsha  
550 River basin, *Earth Syst. Sci. Data*, 11(4), 1711-1744, 2019.

551 Shen, Y., Xiong, A., Wang, Y., and Xie, P.: Performance of high-resolution satellite  
552 precipitation products over China, *J. Geophys. Res.: Atmos.*, 115(D2), 2010.

553 Shen, Y., Zhao, P., Pan, Y., and Yu, J.: A high spatiotemporal gauge–satellite merged  
554 precipitation analysis over China, *J. Geophys. Res.: Atmos.*, 119(6), 3063-3075,  
555 2014.

556 Shi, P., Bai, X., Kong, F., Fang, J., Gong, D., Zhou, T., Guo, Y., Liu, Y., Dong, W.,  
557 Wei, Z., He, C., Yu, D., Wang, J., Ye, Q., Yu, R., and Chen, D.: Urbanization  
558 and air quality as major drivers of altered spatiotemporal patterns of heavy  
559 rainfall in China, *Landscape Ecol.*, 32(8), 1723-1738, 2017.

560 Sloughter, J.M., Raftery, A.E., Gneiting, T., and Fraley, C.: Probabilistic Quantitative  
561 Precipitation Forecasting Using Bayesian Model Averaging. *Mon. Weather Rev.*,  
562 135(9), 3209-3220, 2007.

563 Smith, C.D., Yang, D., Ross, A., and Barr, A.: The Environment and Climate Change  
564 Canada solid precipitation intercomparison data from Bratt's Lake and Caribou  
565 Creek, Saskatchewan, *Earth Syst. Sci. Data*, 11(3), 1337-1347, 2019.

566 Su, F., Hong, Y., and Lettenmaier, D.P.: Evaluation of TRMM Multisatellite

567      Precipitation Analysis (TMPA) and its utility in hydrologic prediction in the La  
568      Plata Basin, *J. Hydrometeorol.*, 9(4), 622-640, 2008.

569      Sun, Q., Miao, C., Duan, Q., Ashouri, H., Soroosh, S., and Hsu, K.: A review of  
570      global precipitation data sets: Data sources, estimation, and intercomparisons,  
571      *Rev. Geophys.*, 56(1), 79-107, 2018.

572      Tong, K., Su, F., Yang, D., and Hao, Z.: Evaluation of satellite precipitation retrievals  
573      and their potential utilities in hydrologic modeling over the Tibetan Plateau, *J.*  
574      *Hydrol.*, 519, 423-437, 2014.

575      Verma, K., and Katpatal, Y.B.: Groundwater monitoring using GRACE and GLDAS  
576      data after downscaling within basaltic aquifer system, *Groundwater*, 2019.

577      Wang, F., Wang, L., Koike, T., Zhou, H., Yang, K., Wang, A., and Li, W.: Evaluation  
578      and application of a fine-resolution global data set in a semiarid mesoscale river  
579      basin with a distributed biosphere hydrological model, *J. Geophys. Res.: Atmos.*,  
580      116(D21), 2011.

581      Wang, L., and Koike, T.: Comparison of a distributed biosphere hydrological model  
582      with GBHM, *Annual Journal of Hydraulic Engineering-JSCE*, 53, 103-108,  
583      2009a.

584      Wang, L., Koike, T., Yang, K., and Yeh, P.J.: Assessment of a distributed biosphere  
585      hydrological model against streamflow and MODIS land surface temperature in  
586      the upper Tone River Basin, *J. Hydrol.*, 377(1-2), 21-34, 2009b.

587      Wang, L., Sun, L., Shrestha, M., Li, X., Liu, W., Zhou, J., Yang, K., Lu, H., and Chen,  
588      D.: Improving snow process modeling with satellite-based estimation of

589 near-surface-air-temperature lapse rate, *J. Geophys. Res.: Atmos.*, 121(20),  
590 12005-12030, 2016.

591 Wang, L., Zhou, J., Qi, J., Sun, L., Yang, K., Tian, L., Lin, Y., Liu, W., Shrestha, M.,  
592 Xue, Y., Koike, T., Ma, Y., Li, X., Chen, Y., Chen, D., Piao, S., and Lu, H.:  
593 Development of a land surface model with coupled snow and frozen soil physics,  
594 *Water Resour. Res.*, 53(6), 5085-5103, 2017a.

595 Wang, S., Liu, J., Wang, J., Qiao, X., and Zhang, J.: Evaluation of GPM IMERG  
596 V05B and TRMM 3B42V7 Precipitation products over high mountainous  
597 tributaries in Lhasa with dense rain gauges, *Remote Sens.*, 11(18), 2080, 2019a.

598 Wang, Y., Chen, J., and Yang, D.: Bayesian assimilation of multiscale precipitation  
599 data and sparse ground gauge observations in mountainous areas, *J.*  
600 *Hydrometeorol.*, 20(8), 1473-1494, 2019b.

601 Wang, Y., Wang, L., Li, X., and Chen, D.: Temporal and spatial changes in estimated  
602 near-surface air temperature lapse rates on Tibetan Plateau, *Int. J. Climatol.*,  
603 38(7), 2907-2921, 2018.

604 Wang, Y., Wang, L., Li, X., and Zhou, J.: High temporal and spatial resolution  
605 precipitation data of Upper Brahmaputra River Basin (1981-2016), Zenodo,  
606 <http://doi.org/10.5281/zenodo.3711155>, 2020.

607 Wang, Y., Yang, H., Yang, D., Qin, Y., Gao, B., and Cong, Z.: Spatial Interpolation  
608 of Daily Precipitation in a High Mountainous Watershed based on Gauge  
609 Observations and a Regional Climate Model Simulation, *J. Hydrometeorol.*,  
610 18(3), 845-862, 2017b.

611 Xia, T., Wang, Z., and Zheng, H.: Topography and data mining based methods for  
612 improving satellite precipitation in mountainous areas of China, *Atmosphere*,  
613 6(8), 983-1005, 2015.

614 Xia, Y., Hao, Z., Shi, C., Li, Y., Meng, J., Xu T., Wu, X., and Zhang B.: Regional and  
615 Global Land Data Assimilation Systems: Innovations, Challenges, and Prospects,  
616 *J. Meteorol. Res.*, 33(2), 159-189, 2019.

617 Xia, Y., Mocko, D.M., Wang, S., Pan, M., Kumar, S.V., Peters-Lidard, C.D., Wei, H.,  
618 Wang, D., and Ek, M.B.: Comprehensive evaluation of the variable infiltration  
619 capacity (VIC) model in the North American Land Data Assimilation System, *J.*  
620 *Hydrometeorol.*, 19(11), 1853-1879, 2018.

621 Xu, R., Tian, F., Yang, L., Hu, H., Lu, H., and Hou, A.: Ground validation of GPM  
622 IMERG and TRMM 3B42V7 rainfall products over southern Tibetan Plateau  
623 based on a high-density rain gauge network, *J. Geophys. Res.: Atmos.*, 122(2),  
624 910-924, 2017.

625 Xue, B., Wang, L., Yang, K., Tian, L., Qin, J., Chen, Y., Zhao, L., Ma, Y., Koike, T.,  
626 Hu, Z., and Li, X.: Modeling the land surface water and energy cycles of a  
627 mesoscale watershed in the central Tibetan Plateau during summer with a  
628 distributed hydrological model, *J. Geophys. Res.: Atmos.*, 118(16), 8857-8868,  
629 2013.

630 Yang, K., He, J., Tang, W., Qin, J., and Chen, C.C.K.: On downward shortwave and  
631 longwave radiations over high altitude regions: observation and modeling in the  
632 Tibetan Plateau, *Agr. Forest Meteorol.*, 150(1), 38-46, 2010.

633 Yang, K., Wu, H., Qin, J., Lin, C., Tang, W., and Chen, Y.: Recent climate changes  
634 over the Tibetan Plateau and their impacts on energy and water cycle: A review,  
635 Global Planet. Change, 112, 79-91, 2014.

636 Yi, X., Li, G., and Yin, Y.: Spatio-temporal variation of precipitation in the  
637 Three-River Headwater Region from 1961 to 2010, J. Geogr. Sci., 23(3),  
638 447-464, 2013.

639 Yong, B., Liu, D., Gourley, J.J., Tian, Y., Huffman, G.J., Ren, L., and Hong, Y.:  
640 Global view of real-time TRMM multisatellite precipitation analysis:  
641 Implications for its successor global precipitation measurement mission, Bull.  
642 Am. Meteorol. Soc., 96(2), 283-296, 2015.

643 Zaitchik, B.F., Rodell, M., and Olivera, F.: Evaluation of the Global Land Data  
644 Assimilation System using global river discharge data and a source-to-sink  
645 routing scheme, Water Resour. Res., 46(6), 2010.

646 Zhang, Q., Shi, P., Singh, V.P., Fan, K., and Huang, J.: Spatial downscaling of  
647 TRMM - based precipitation data using vegetative response in Xinjiang, China,  
648 Int. J. Climatol., 37(10), 3895-3909, 2017.

649 Zhou, J., Wang, L., Zhang, Y., Guo, Y., Li, X., and Liu, W.: Exploring the water  
650 storage changes in the largest lake (Selin Co) over the Tibetan Plateau during  
651 2003–2012 from a basin-wide hydrological modeling, Water Resour. Res.,  
652 51(10), 8060-8086, 2015a.

653 Zhou, Y., Lau, W.K.M., and Huffman, G.J.: Mapping TRMM TMPA into average  
654 recurrence interval for monitoring extreme precipitation events, J. Appl.

655 Meteorol. Clim., 54(5), 979-995, 2015b.

656

657 **Table and figure captions**

658 **Table 1.** The precipitation products used in this study.

659 **Figure 1.** The Upper Brahmaputra River Basin originates from the Tibetan Plateau  
660 (TP) with the spatial distribution of nine meteorological stations from the China  
661 Meteorological Administration (CMA) and 166 rain gauges from Ministry of Water  
662 Resources (MWR), China. The green arrow indicates the direction of the westerlies,  
663 the Indian monsoon and the East Asian monsoon. The elevation data was obtained  
664 from the SRTM DEM datasets ([www.earthexplorer.usgs.gov](http://www.earthexplorer.usgs.gov)).

665 **Figure 2.** The flowchart used to produce the spatio-temporal continuous precipitation  
666 dataset ( $P_{int}$ ).

667 **Figure 3.** The spatial distribution of  $P_{int}$  (mm) averaged from 1981 to 2016 (a.  
668 annual; b. seasonal).

669 **Figure 4.** The spatial distribution of different precipitation products during the warm  
670 season (May to October) and the cold season (November to April) averaged from  
671 2008 to 2016.

672 **Figure 5.** Variations in basin-averaged precipitation from multi-year monthly mean  
673 values (top), annual values (middle) and monthly values (bottom) for the different  
674 products.

675 **Figure 6.** A comparison of the probability distribution function (PDF) between all the  
676 monthly observations and different precipitation products in the warm seasons (May  
677 to October in 2014 and 2016).

678 **Figure 7.** As for Figure 6 but with scatter plots.

679 **Figure 8.** A validation of  $P_{int}$  against short time series by comparing with daily  
680 gauge-averaged precipitation from May to October in 2014 and 2016.

681 **Figure 9.** A validation of  $P_{int}$  (mm) against short time series: spatial distribution of  
682 the observations and corresponding grids in  $P_{int}$  from May to October in 2014 and  
683 2016.

684 **Figure 10.** A validation of  $P_{int}$  against a long time series: (a). PDF and scatter plots  
685 for monthly precipitation at nine CMA stations, (b). station-averaged monthly  
686 precipitation from 1981 to 2016.

687 **Figure 11.** A trend analysis of the annual and seasonal precipitation (a: annual; b:  
688 spring; c: summer; d: autumn; e: winter) over 36 years (1981-2016) between  $P_{int}$ ,  
689 GLDAS, ITP-Forcing and MERRA2. The triangles represent the observed trend of  
690 the corresponding meteorological stations.

691 **Figure 12.** The number of meteorological stations (total of nine) which present the  
692 same trends as the different precipitation products, according to Figure 11.

693 **Figure 13.** A comparison of extreme events, as captured by different precipitation  
694 products.

695 **Figure 14.** An evaluation of simulated daily discharge at Nuxia station from 2008 to  
696 2016 forced by different precipitation products. All the discharge values have been  
697 normalized.

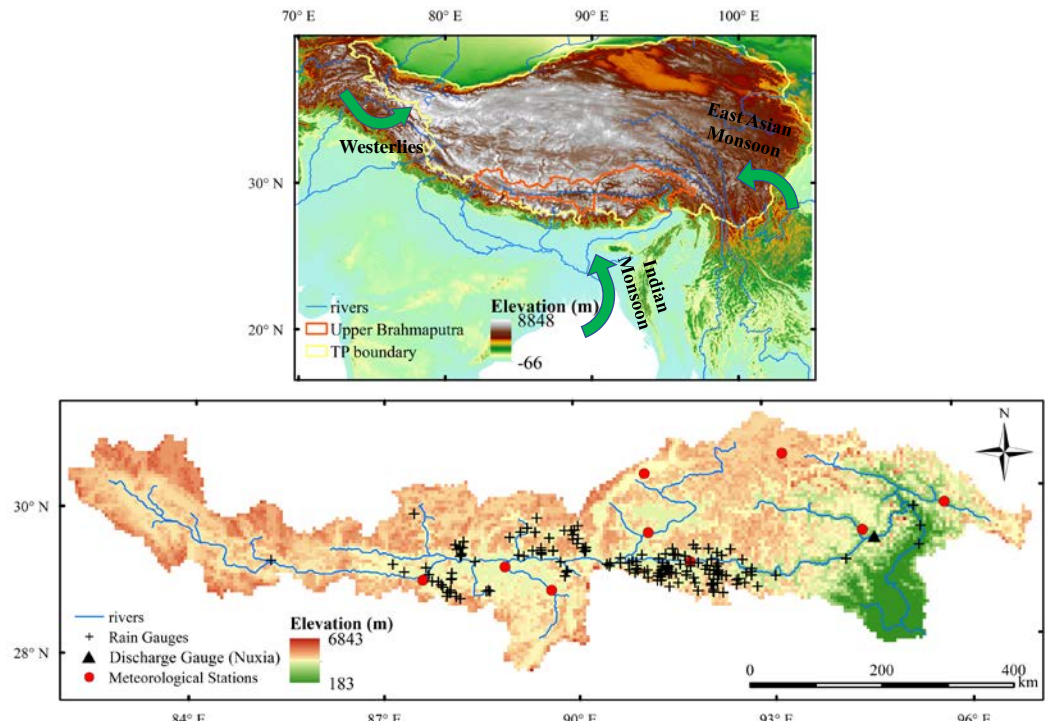
698

699 **Table 1.** The precipitation products used in this study.

Precipitation products	Time range	Temporal resolution	Spatial resolution
CMA gridded data	2008-2016	hourly	$0.1^\circ \times 0.1^\circ$
GLDAS	1981-2016	3-hour	$0.25^\circ \times 0.25^\circ$
ITP-Forcing	1981-2016	3-hour	$0.1^\circ \times 0.1^\circ$
MERRA2	1981-2016	hourly	$0.5^\circ \times 0.625^\circ$
TRMM	1998-2016	3-hour	$0.25^\circ \times 0.25^\circ$

700

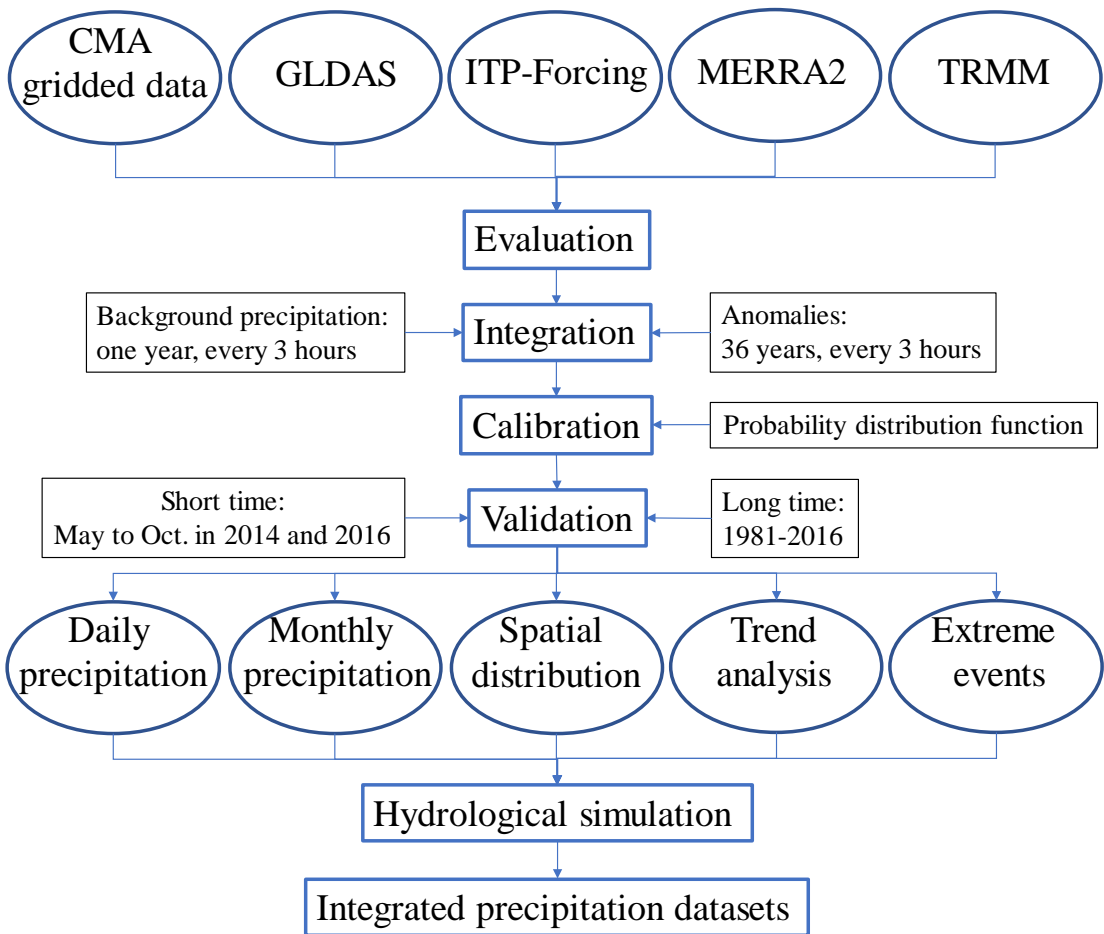
701



702

703 **Figure 1.** The Upper Brahmaputra River Basin originates from the Tibetan Plateau  
 704 (TP) with the spatial distribution of nine meteorological stations from the China  
 705 Meteorological Administration (CMA) and 166 rain gauges from Ministry of Water  
 706 Resources (MWR), China. The green arrow indicates the direction of the westerlies,  
 707 the Indian monsoon and the East Asian monsoon. The elevation data was obtained  
 708 from the SRTM DEM datasets ([www.earthexplorer.usgs.gov](http://www.earthexplorer.usgs.gov)).

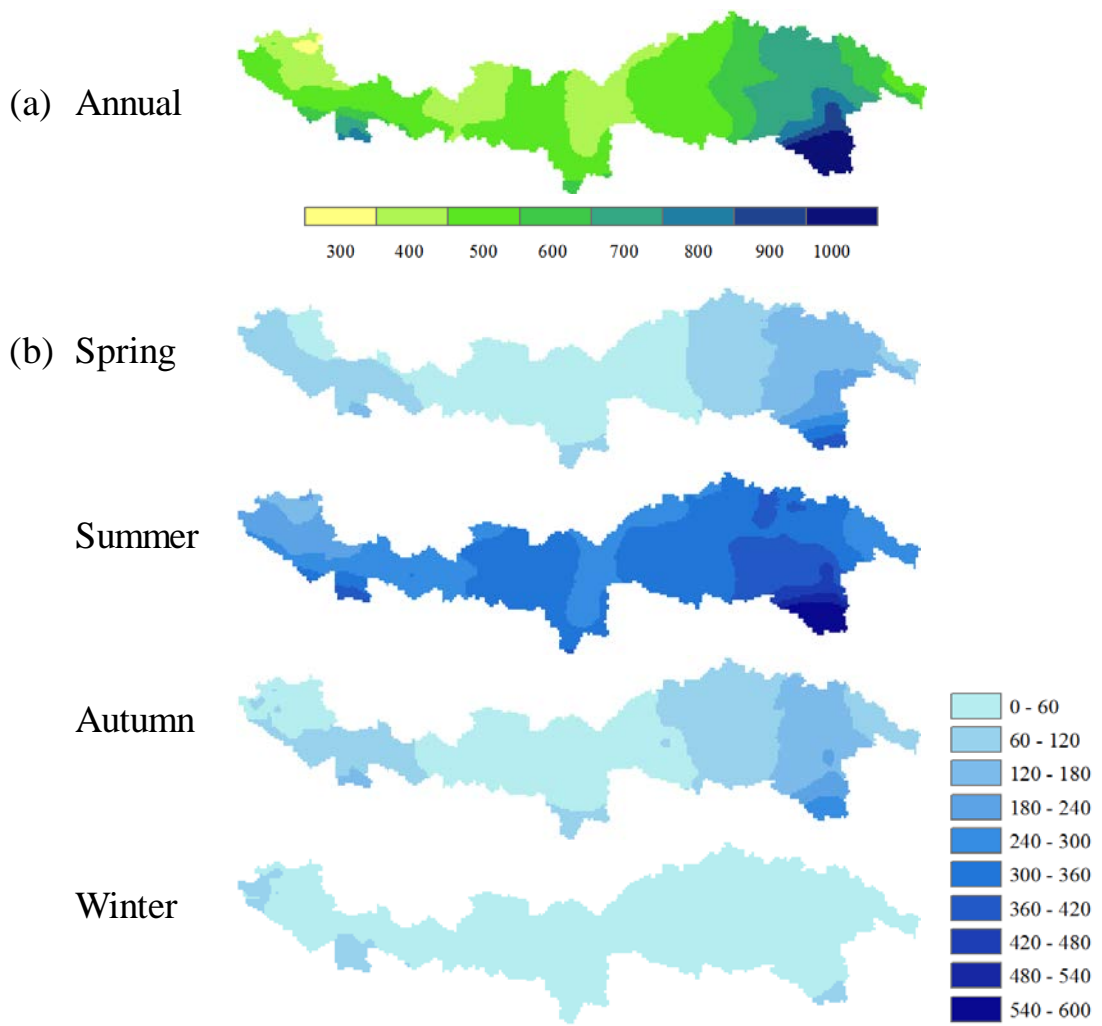
709



710

711 **Figure 2.** The flowchart used to produce the spatio-temporal continuous precipitation  
 712 dataset ( $P_{int}$ ).

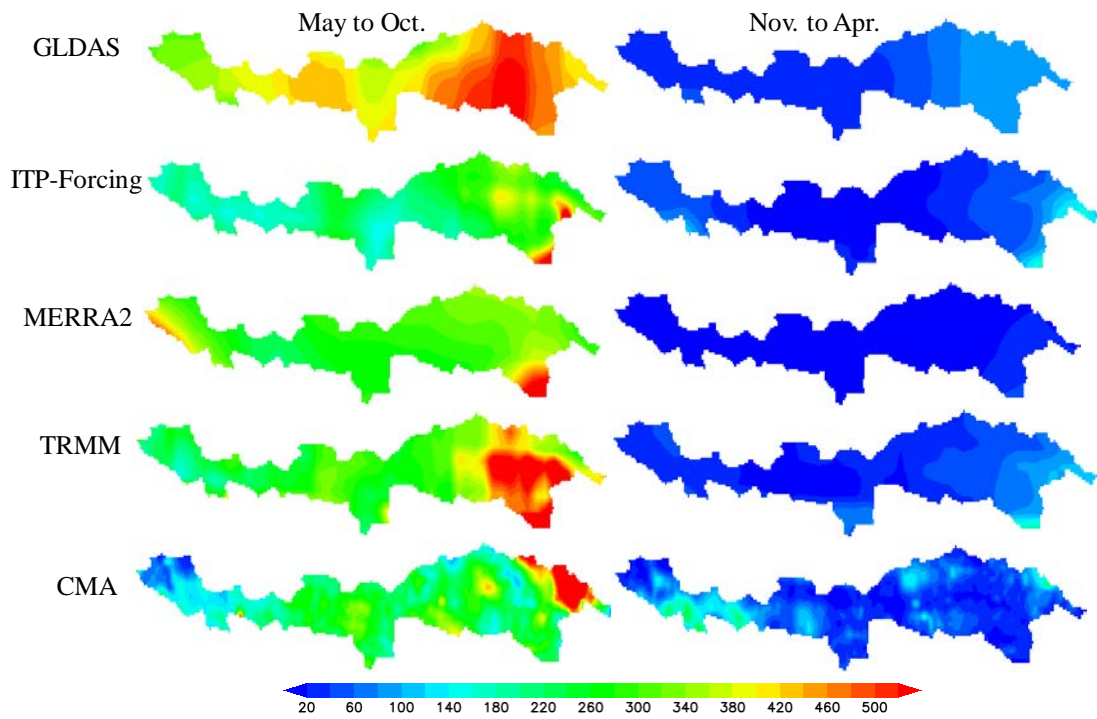
713



714

715 **Figure 3.** The spatial distribution of  $P_{int}$  (mm) averaged from 1981 to 2016 (a.  
 716 annual; b. seasonal).

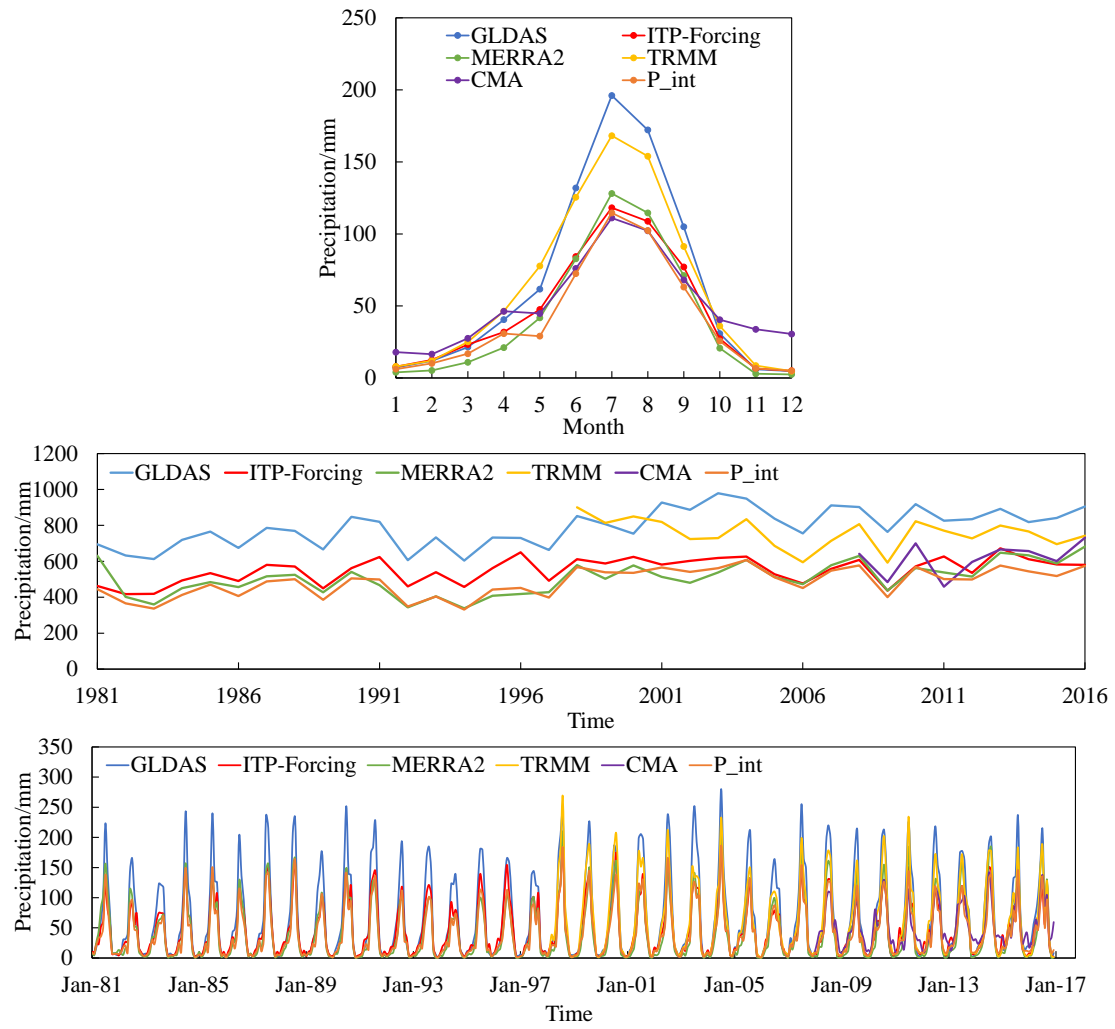
717



718

719 **Figure 4.** The spatial distribution of different precipitation products during the warm  
720 season (May to October) and the cold season (November to April) averaged from  
721 2008 to 2016.

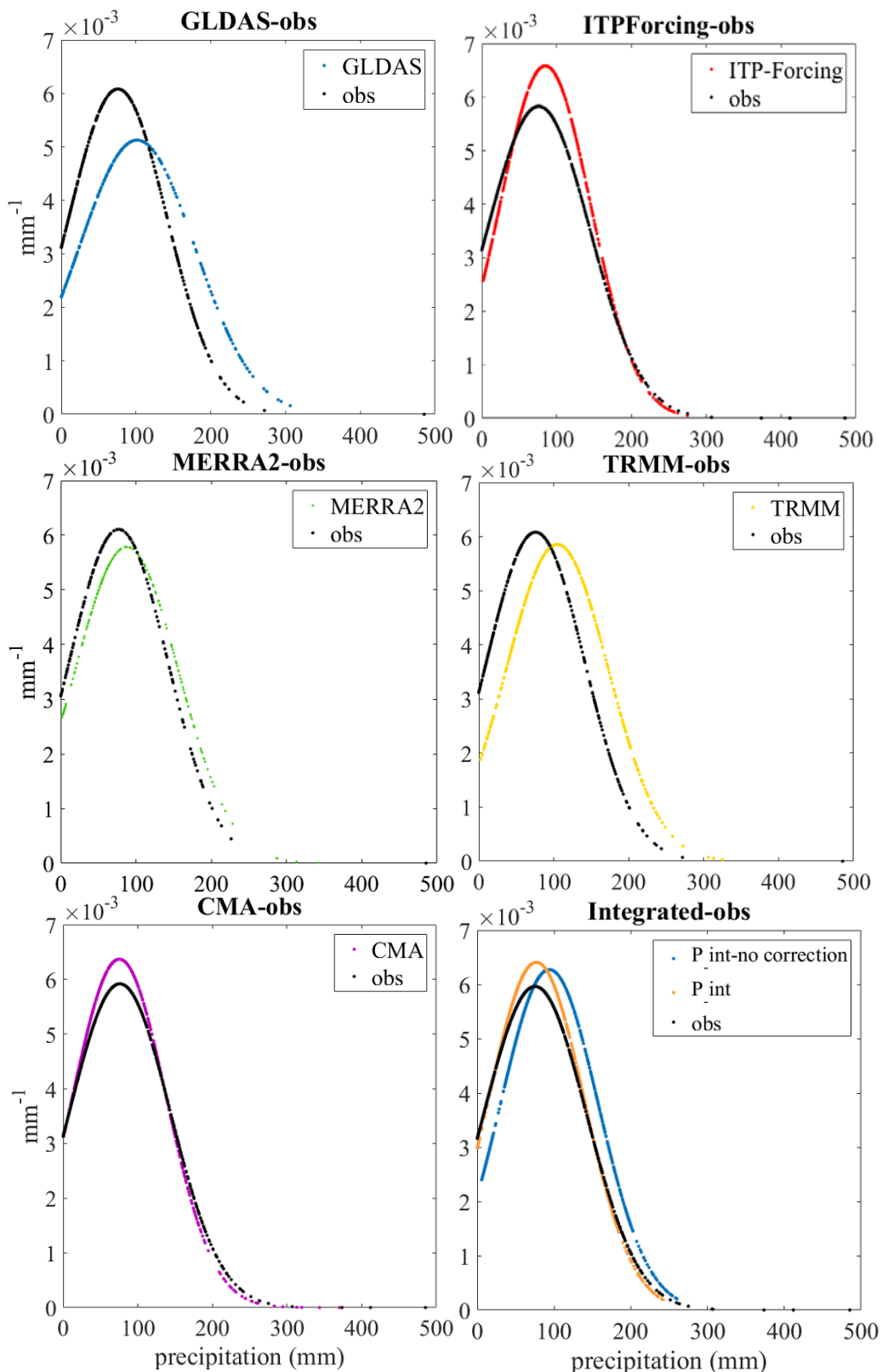
722



723

724 **Figure 5.** Variations in basin-averaged precipitation from multi-year monthly mean  
 725 values (top), annual values (middle) and monthly values (bottom) for the different  
 726 products.

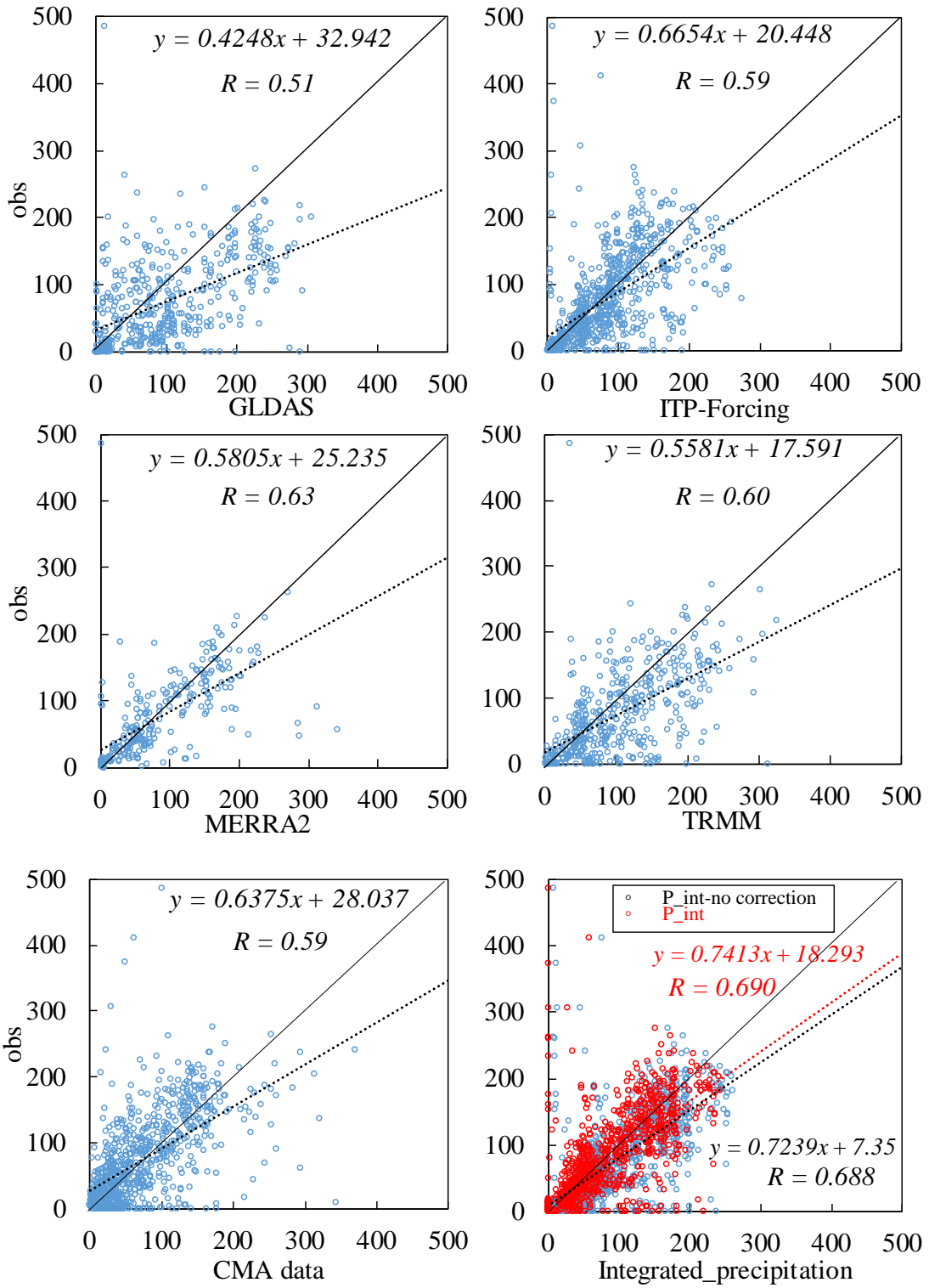
727



728

729 **Figure 6.** A comparison of the probability distribution function (PDF) between all the  
 730 monthly observations and different precipitation products in the warm seasons (May

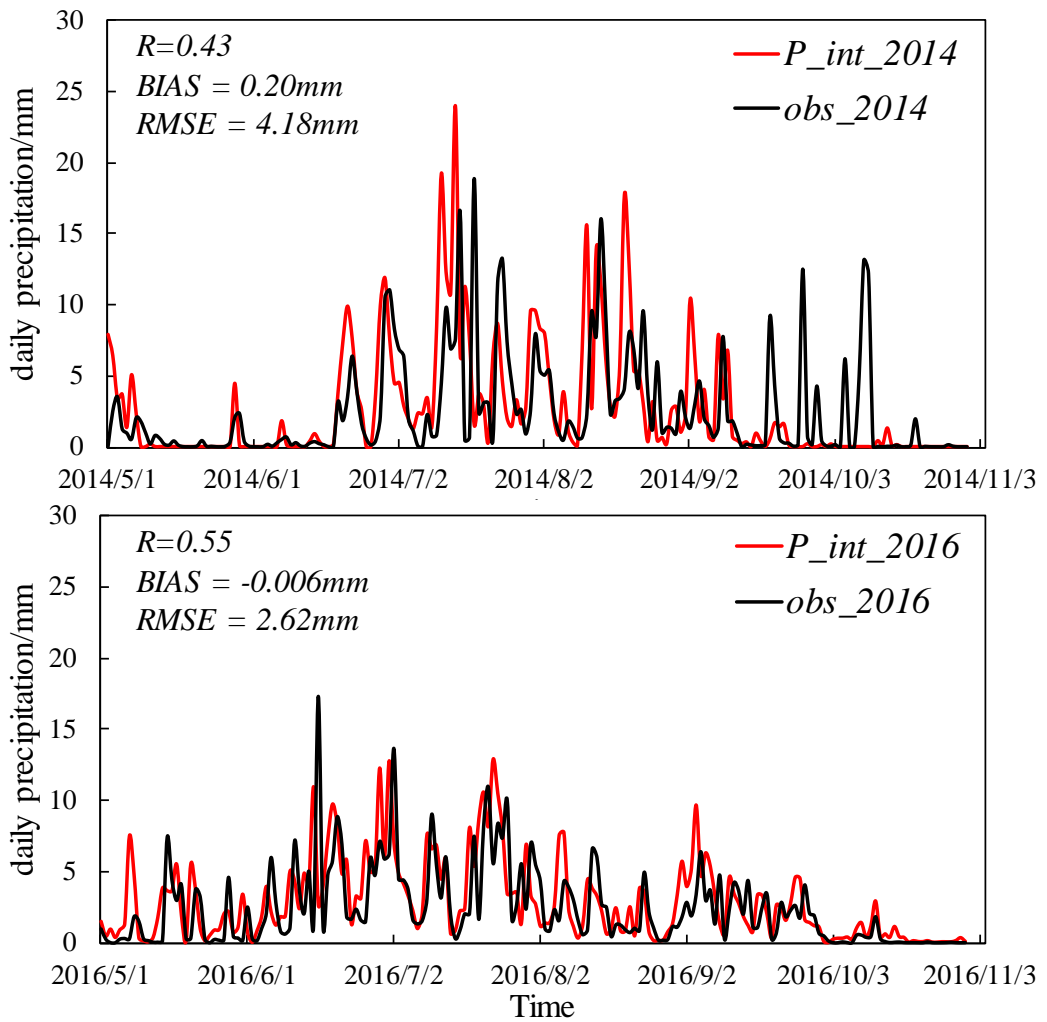
731 to October in 2014 and 2016).



732

733

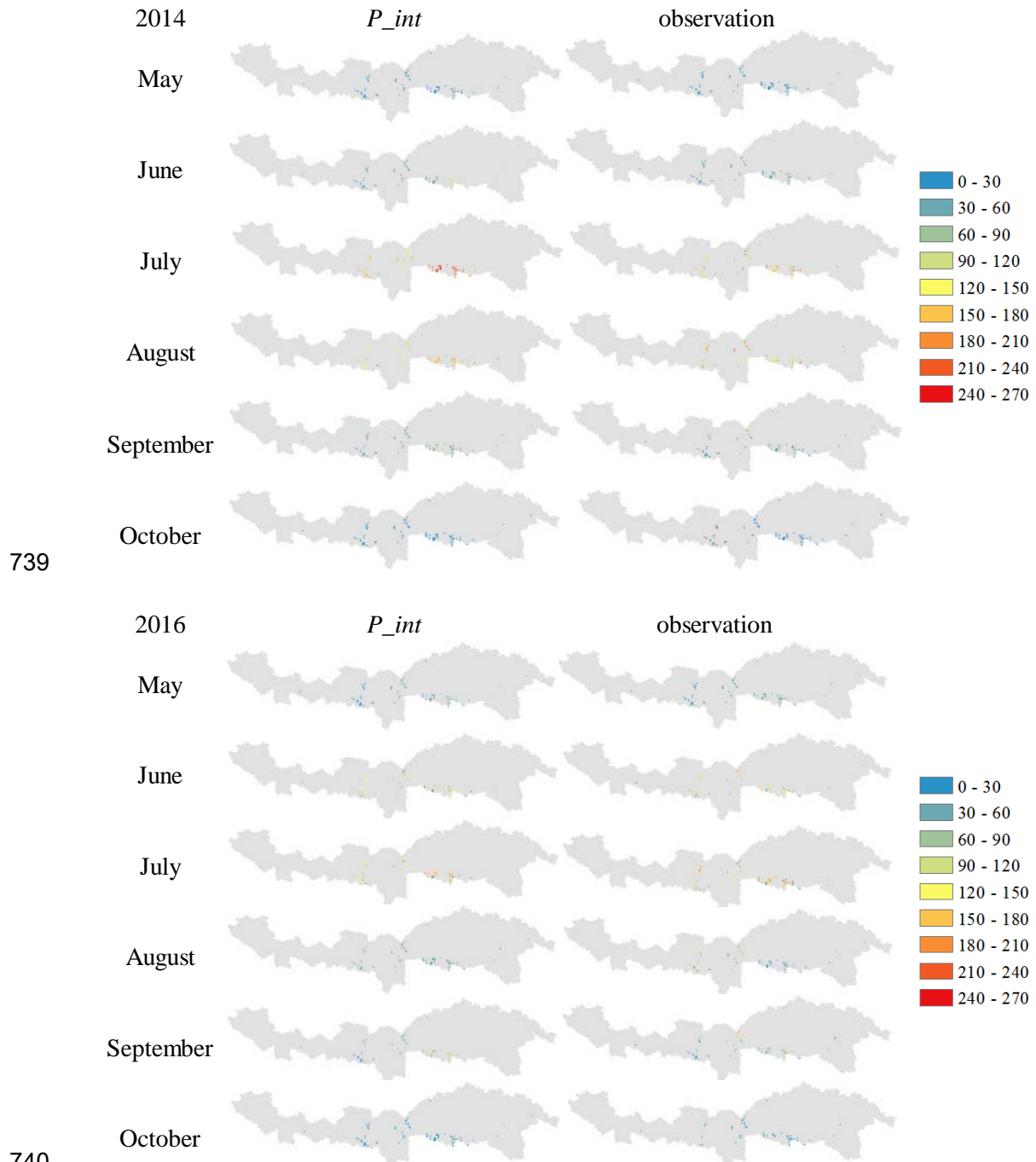
734 **Figure 7.** As for Figure 6 but with scatter plots.



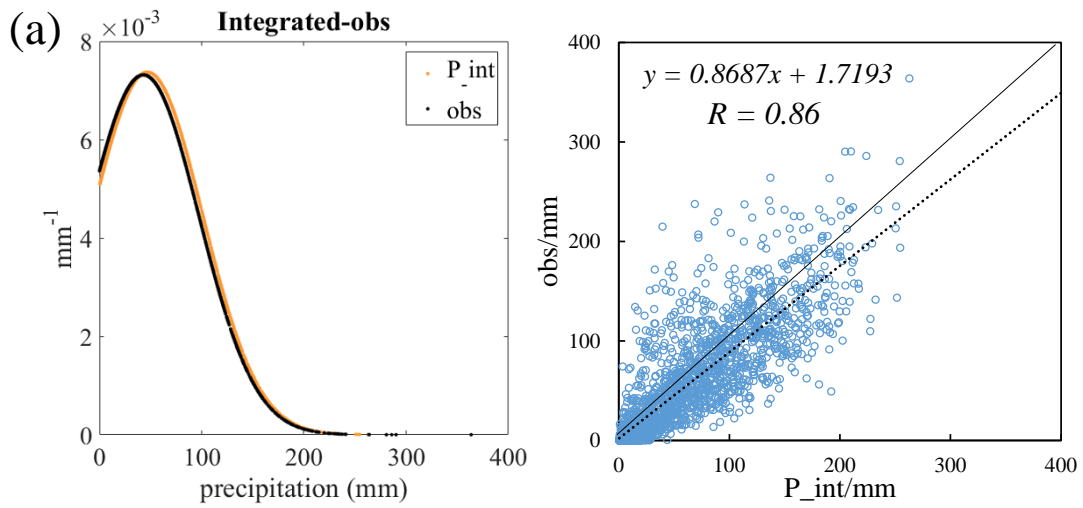
735

736 **Figure 8.** A validation of  $P_{int}$  against short time series by comparing with daily  
 737 gauge-averaged precipitation from May to October in 2014 and 2016.

738



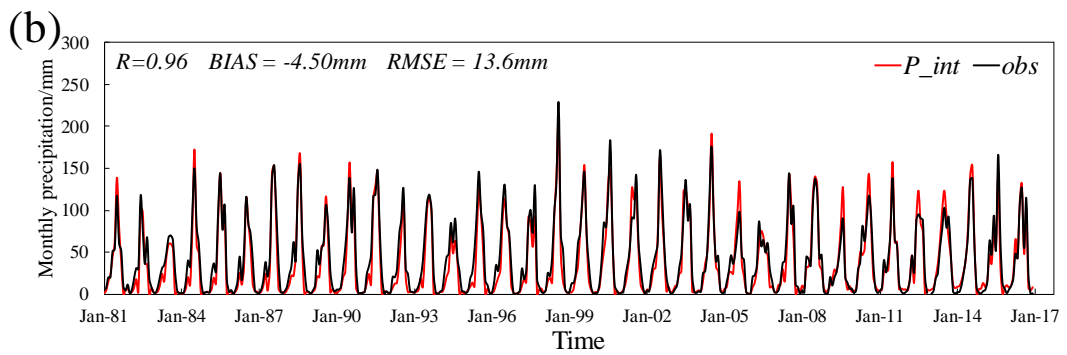
744



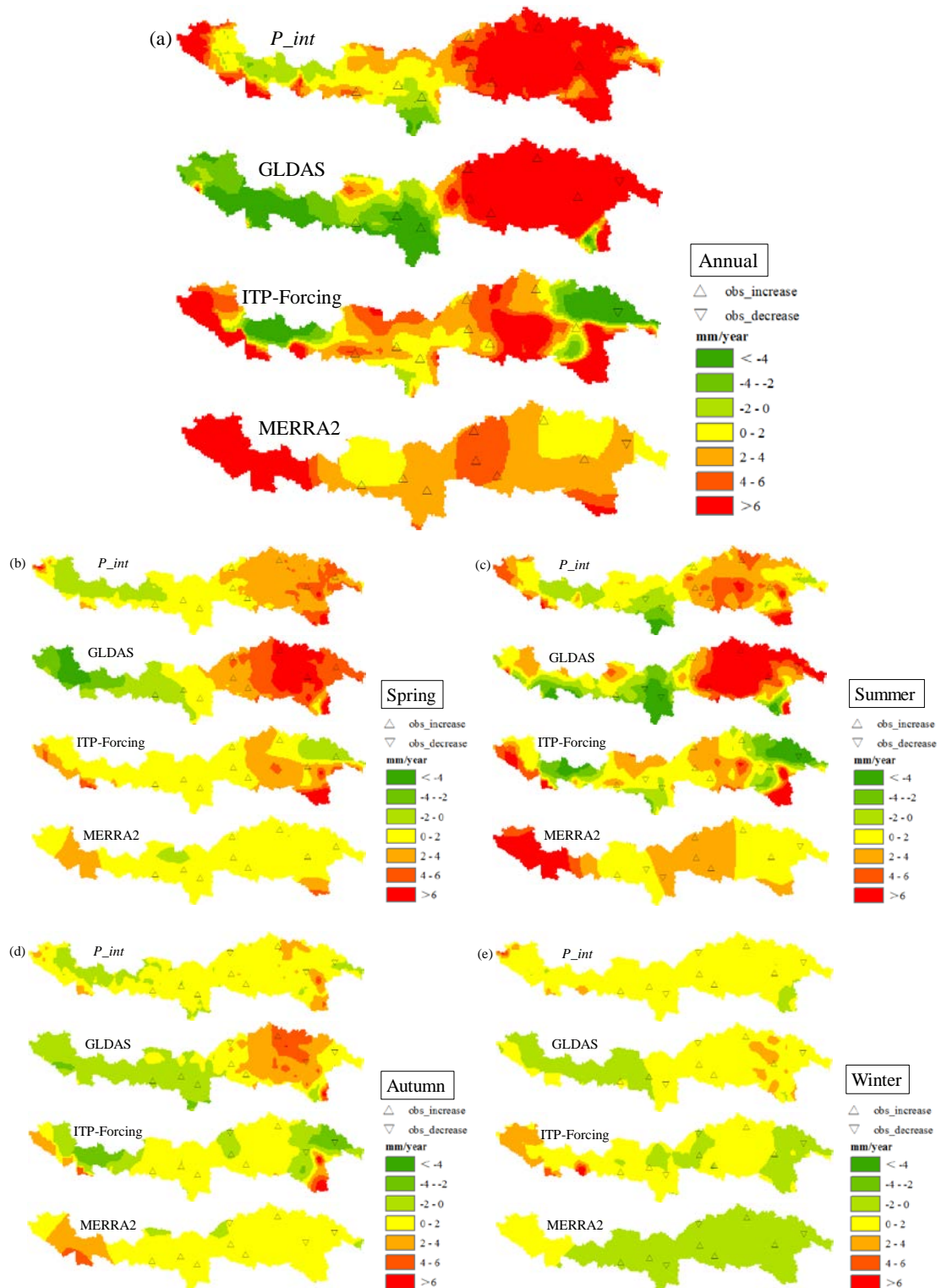
745

746 **Figure 10.** A validation of  $P_{int}$  against a long time series: (a). PDF and scatter plots  
 747 for monthly precipitation at nine CMA stations, (b). station-averaged monthly  
 748 precipitation from 1981 to 2016.

749



750

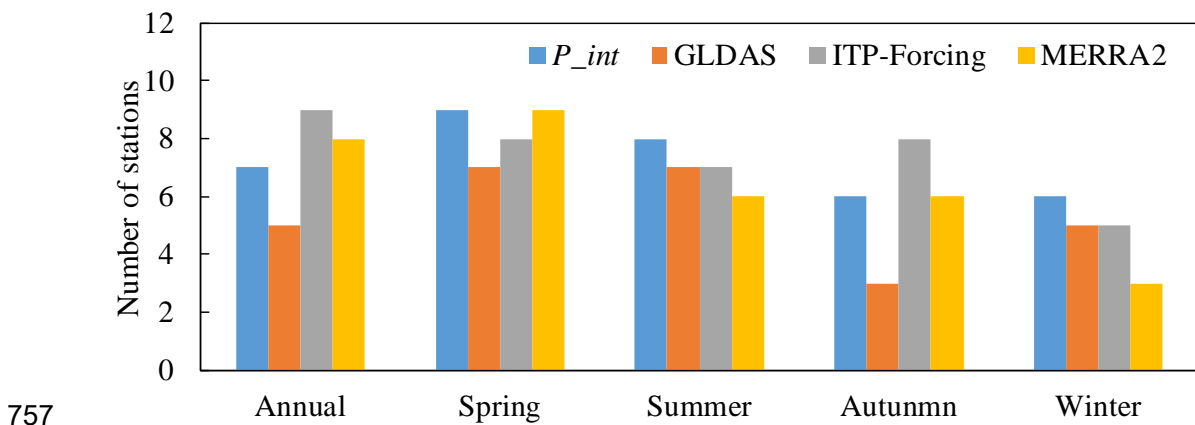


751

752

753 **Figure 11.** A trend analysis of the annual and seasonal precipitation (a: annual; b:  
754 spring; c: summer; d: autumn; e: winter) over 36 years (1981-2016) between  $P_{int}$ ,  
755 GLDAS, ITP-Forcing and MERRA2. The triangles represent the observed trend of

756 the corresponding meteorological stations.

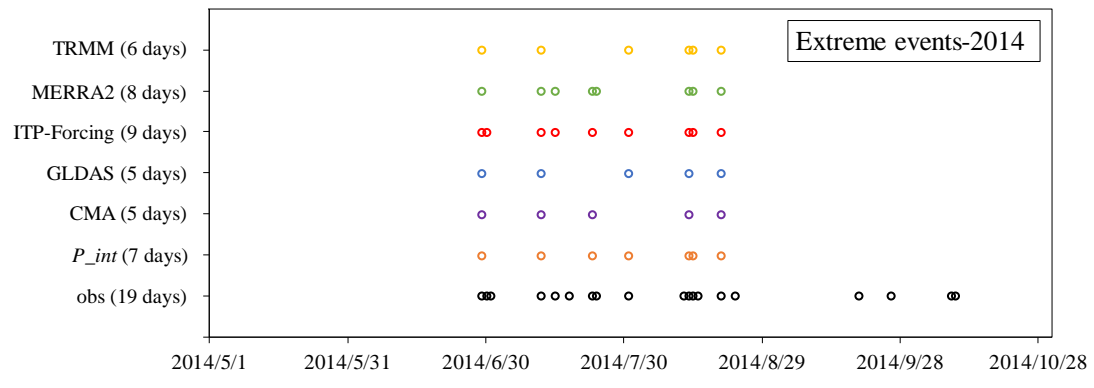


757 **Figure 12.** The number of meteorological stations (total of nine) which present the

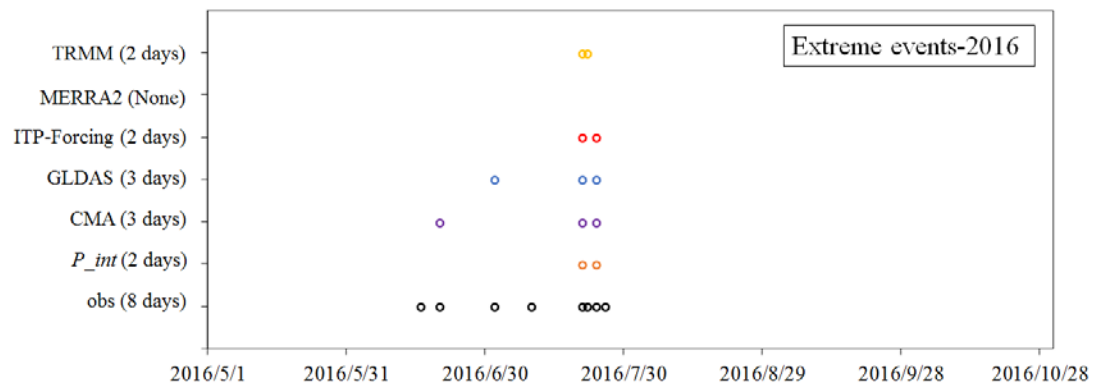
758 same trends as the different precipitation products, according to Figure 11.

760

761



762



763

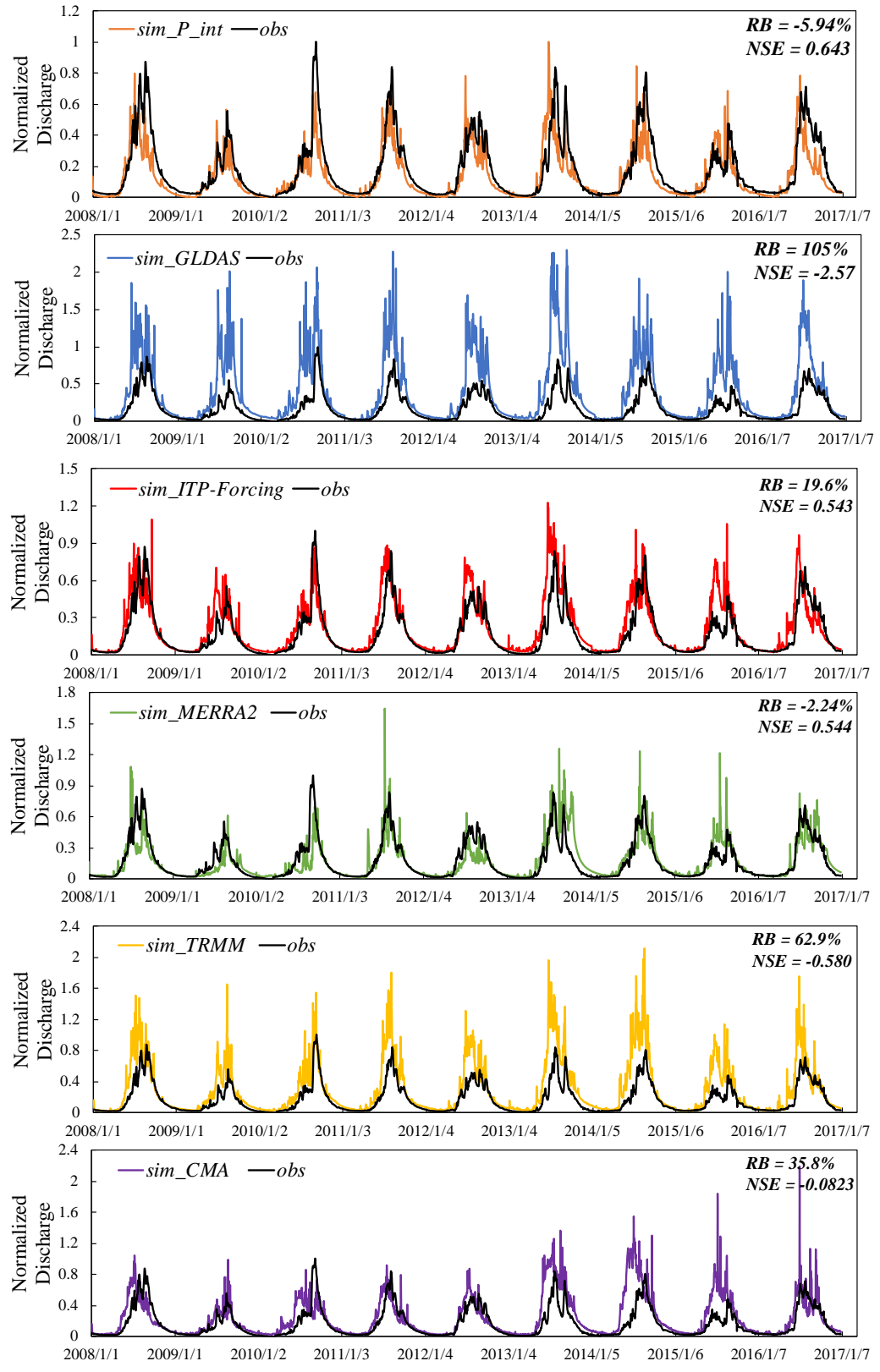
**Figure 13.** A comparison of extreme events, as captured by different precipitation

764

products.

765

766



767

768

769 **Figure 14.** An evaluation of simulated daily discharge at Nuxia station from 2008 to  
 770 2016 forced by different precipitation products. All the discharge values have been

771 normalized.